Annu. Rev. Astron. Astrophys. 1996. 34:279–329

INTERSTELLAR ABUNDANCES FROM ABSORPTION-LINE OBSERVATIONS WITH THE *HUBBLE SPACE TELESCOPE*

Blair D. Savage

Department of Astronomy, University of Wisconsin, Madison, Wisconsin 53706

Kenneth R. Sembach

Center for Space Research, Massachusetts Institute of Technology, Cambridge, Massachusetts 02139

KEY WORDS: interstellar gas, interstellar dust, halo gas, ultraviolet spectra

ABSTRACT

The Goddard High-Resolution Spectrograph (GHRS) aboard the *Hubble Space Telescope* (*HST*) has yielded precision abundance results for a range of interstellar environments, including gas in the local medium, in the warm neutral medium, in cold diffuse clouds, and in distant halo clouds. Through GHRS studies, investigators have determined the abundances of elements such as C, N, O, Mg, Si, S, and Fe in individual interstellar clouds. These studies have provided new information about the composition of interstellar dust grains, the origin of the Galactic high-velocity cloud system, and the processes that transport gas between the disk and the halo. Precision measurements of the interstellar D to H ratio and of the abundances of r- and s-process elements have also provided fiducial reference values for cosmological and stellar evolutionary observations and theoretical models.

0066-4146/96/0915-0279$08.00

1. INTRODUCTION

The absorption lines of most atoms and molecules found in the interstellar medium (ISM) occur at ultraviolet (UV) wavelengths. Their direct detection through absorption-line spectroscopy requires instrumentation above the Earth's atmosphere. The first UV observations of interstellar absorption lines were obtained toward bright O and B stars with small spectrometers carried on sounding rockets (e.g. Morton & Spitzer 1966). These early studies were followed by the 1972 launch of the very successful Princeton telescope-spectrometer on the *Copernicus* satellite (Rogerson et al 1973; for a review of *Copernicus* results see Spitzer & Jenkins 1975). Throughout its 10-year lifetime, the *Copernicus* satellite provided fundamental information about elemental abundances in diffuse interstellar clouds (Cowie & Songaila 1986; Jenkins 1987). During the 1980s many interstellar programs were pursued with the *International Ultraviolet Explorer* (*IUE*) satellite (de Boer et al 1987). The lower spectral resolution of the *IUE* [full width at half maximum (FWHM) ≈ 25 vs 13 km s^{-1}] limited its ability to probe element abundances in the neutral gas as accurately as *Copernicus*, but the *IUE* was used effectively to study interstellar dust (Mathis 1987), atomic hydrogen (Shull & van Steenberg 1985; Diplas & Savage 1994), the highly ionized ISM (Sembach & Savage 1992), gas kinematics (Jenkins 1990), and nebular emissions (Dufour 1987; Köppen & Aller 1987). Very high-resolution far-UV spectra of bright stars have been obtained with the Interstellar Medium Absorption Profile Spectrograph (IMAPS) (Jenkins et al 1988). This instrument was first flown on a sounding rocket (Jenkins et al 1989; Joseph & Jenkins 1991) and was part of the recent ORFEUS-SPAS mission (Jenkins 1995). Precision high-resolution interstellar absorption-line spectroscopy was greatly enhanced with the launch of the Goddard High-Resolution Spectrograph (GHRS) aboard the *Hubble Space Telescope* (*HST*) in 1990. In this review we discuss many of the ISM abundance results obtained through GHRS absorption-line observations. We also discuss a few interstellar absorption-line results from the *HST* Faint Object Spectrograph (FOS). However, because of its relatively low resolution (~ 300 km s^{-1}), the FOS is more useful for studies of the emission from interstellar gas, which is not the subject of this review. The recent review of light elements and isotope ratios by Wilson & Rood (1994) complements the results discussed in this paper.

Measures of ISM elemental abundances provide important information about the physical conditions, chemical composition, and Galactic evolution of the gaseous material in the Milky Way. Heavy elements regulate gas temperatures through a variety of interstellar heating and cooling processes. The formation rates of molecules through gas-phase chemistry or on grain surfaces depend on the abundances of the reacting species. Many heavy elements have gas

phase abundances that are less than the expected cosmic abundances because of varying levels of incorporation into interstellar dust grains. This phenomenon is referred to as depletion.

Gas-phase abundance measurements provide the most direct way by which to obtain information about elemental depletion in different Galactic environments and to gain insight into the composition of interstellar grains and the exchange of matter between the gaseous and solid forms through depletion and grain destruction processes (Jenkins 1987; Mathis 1990). Absolute interstellar abundances (gas + dust) serve as fundamental benchmarks for interpretations of abundances in galaxies and gas clouds in the distant Universe. Eventually, comparisons of these Milky Way abundances with those found in high-redshift quasar absorption-line systems will enable astronomers to study elemental abundance evolution over approximately 90% of the age of the Universe.

2. UV ABSORPTION-LINE DIAGNOSTICS

Ground-based optical absorption-line observations of interstellar gas are limited to a few molecules and a small number of ions from elements of relatively low cosmic abundance. Species observed from the ground include the atoms Li I, Na I, Ca I, Ca II, K I, Fe I, and Ti II and the molecules CH, CH^+, CN, C_2, and NH. In contrast, Table 1 lists the atomic and molecular species with resonance or low-excitation energy lines in the 1150 to 3200 Å region, as detected by the GHRS. Access to UV wavelengths allows the direct detection of absorption by such abundant atoms as C, N, O, Mg, Si, and Fe in a number of ionization states, including those found in cool neutral gas (C I, C II, N I, O I, etc) and in the hot ISM (C IV and N V). Adjacent ionization stages in the UV of the same element are useful for determining physical and ionization conditions in the gas because the ionic ratios for a given element do not depend on assumptions about relative elemental abundances. Examples of adjacent ions are C I-II, Mg I-II, Si I-II-III-IV, S I-II-III, and P I-II-III. UV observations also make possible studies of rare isotopes (i.e. D) and of elements of low cosmic abundance such as B, Ga, Ge, As, Se, Kr, Sn, Te, Tl, and Pb. An understanding of the abundances of these species may lead to information about primordial nucleosynthesis occurring in the Big Bang and about the enrichment of the interstellar gas with heavy elements created through both slow and rapid neutron capture processes.

The GHRS can perform sensitive searches for interstellar molecules that provide insights into interstellar chemical processes. Important molecules with lines in the accessible wavelength region include CH_2, CO, C_2, CO^+, N_2, CN^+, NO, NO^+, H_2O, OH, MgH^+, SiO, CS, and HCl. Molecules already detected are listed at the bottom of Table 1. Studies of abundant molecules such as CO are valuable in investigating interstellar isotopic abundances, the role of chemical

Table 1 Atoms and molecules with absorption lines detected in the ISM with the GHRS

Atoms[a] (1150 < λ < 3200 Å)	Z[b]	IP(eV)[c] (I to II)	IP(eV)[c] (II to III)	$\log(X/H)_m + 12$[d]
H I	1	13.60	...	12.00
D I	1	13.60	...	....
B II	5	8.30	25.15	2.88±0.04
C I, C I*, C I**, C II, C II*, C IV	6	11.26	24.38	8.55±0.05
N I, N V	7	14.53	29.60	7.97±0.07
O I, O I*	8	13.62	35.12	8.87±0.07
Mg I, Mg II	12	7.65	15.04	7.58±0.02
Al II, Al III	13	5.99	18.83	6.48±0.02
Si I, Si II, Si II*, Si III, Si IV	14	8.15	16.35	7.55±0.02
P I, P II, P III	15	10.49	19.73	5.57±0.04
S I, S II, S III	16	10.36	23.33	7.27±0.05
Cl I	17	12.97	23.81	5.27±0.06
Cr II	24	6.77	16.50	5.68±0.03
Mn II	25	7.44	15.64	5.53±0.04
Fe II	26	7.87	16.18	7.51±0.01
Co II	27	7.86	17.06	4.91±0.03
Ni II	28	7.64	18.17	6.25±0.02
Cu II	29	7.73	20.29	4.27±0.05
Zn II	30	9.39	17.96	4.65±0.02
Ga II	31	6.00	20.51	3.13±0.03
Ge II	32	7.90	15.93	3.63±0.04
As II	33	9.81	18.63	2.37±0.05
Sc II	34	9.75	21.19	3.35±0.03
Kr I	36	14.00	24.36	3.23±0.07
Sn II	50	7.34	14.63	2.14±0.04
Tl II	81	6.11	20.43	0.82±0.04
Pb II	82	7.42	15.03	2.05±0.03

Molecules: $H_2(v = 3)$, OH, ^{12}CO, ^{13}CO, $C^{17}O$, $C^{18}O$, C_2, HCl

[a]The dominant ions found in neutral H regions are underlined. Because little ionizing radiation with $E > 13.6$ eV occurs in H I regions, the dominant ions are simply determined by whether the first ionization potential IP(I to II) is less than or greater than 13.6 eV. For Cl, C1 I sometimes is the dominant ion in regions containing H I and H_2 since chemical exchange reactions involving, H_2, establish the ionization equilibrium (Jura 1974, Jenkins et al 1986).

[b]Atomic number.

[c]First and second ionization potentials in eV from Moore (1970) are listed.

[d]The Solar System meteoritic abundances are from Anders & Grevesse (1989) except for C, N, and O, which are photospheric values from Grevesse & Noels (1993).

fractionation, and differences in photodestruction rates. Unfortunately, the electronic transitions for the most abundant interstellar molecule, H_2 (in the ground $v'' = 0$ vibration level), occur at wavelengths $\lambda < 1110$ Å, which are inaccessible to the GHRS[1]. As a result, information about this important molecule must be obtained from the *Copernicus* results (Spitzer & Jenkins 1975;

[1]The short-wavelength Digicon detector on the GHRS has a LiF window and can detect wavelengths as short as ∼1070 Å with low efficiency. However, with the addition of the Corrective Optics Space Telescope Axial Replacement (COSTAR) (see next section) and two additional reflections from mirrors with MgF overcoats, the GHRS efficiency at these short wavelengths is very low.

Savage et al 1977). However, the GHRS can record absorption by H_2 from excited vibrational levels, and 2σ detections of the H_2 B-X (0-3) R(0) and R(1) lines at $\lambda\lambda$1274.535 and 1274.922 Å have been reported (Federman et al 1995).

3. THE GODDARD HIGH-RESOLUTION SPECTROGRAPH

The GHRS is the primary first-generation instrument aboard the *HST* for absorption-line studies of the Galactic interstellar gas at UV wavelengths from 1150 to 3200 Å (Brandt et al 1994; Heap et al 1995). The GHRS contains first-order diffraction gratings for low-resolution ($\lambda/\Delta\lambda \approx 2000$; $\Delta v = 150$ km s^{-1}) and intermediate-resolution ($\lambda/\Delta\lambda \approx 20{,}000$; $\Delta v = 15$ km s^{-1}) spectroscopy as well as an echelle grating (in combination with two cross-dispersers) for high-resolution ($\lambda/\Delta\lambda \approx 85{,}000$; $\Delta v = 3.5$ km s^{-1}) spectroscopy. A carousal rotates to bring the desired grating into the optical path and place the wavelength region of interest onto one of two 512-diode linear array photon-counting Digicon detectors.

The GHRS has both large ($2'' \times 2''$) and small ($0.25'' \times 0.25''$) entrance apertures for science observations. During its first two years of operation, spectra obtained with the large aperture had a degraded spectral resolution because of the spherical aberration present in the *HST* 2.4-m primary mirror. Spectra obtained in the small aperture achieved the full spectroscopic resolutions listed above but required integrations approximately three to four times longer than what would have been needed with a non-aberrated mirror because of light loss. The successful Space Shuttle repair and refurbishment mission in December 1993 fixed these problems with the addition of the Corrective Optics Space Telescope Axial Replacement (COSTAR), which provided corrective optics to the GHRS and other *HST* instruments. The post-COSTAR performance of the GHRS (Soderblom et al 1995) is close to the original GHRS design goals except for some loss of sensitivity at the shortest wavelengths.

Compared with previous instruments for UV interstellar studies, the GHRS offers higher spectral resolution, low-noise photon-counting detectors with modest multiplexing capability, and a relatively large aperture (2.4 m) of the *HST* primary mirror. The 3.5-km s^{-1} resolution of the echelle mode permits study of conditions in individual interstellar clouds. With poorer spectral resolution, severe blending can occur because interstellar H I clouds have mean velocity differences of ≈ 6 km s^{-1} (Spitzer 1978). Some interstellar clouds may remain unresolved even at the echelle resolutions offered by the GHRS; high-resolution observations from the ground reveal that velocity structure exists at the level of 1 km s^{-1} in some cold H I clouds (Wayte et al 1978; Blades et al

1980; Welty et al 1994).

The GHRS 512-channel Digicon detectors are capable of very high signal-to-noise (S/N) spectroscopy. The combination of high-resolution and high S/N spectroscopy makes possible searches for elements with low cosmic abundances as well as studies of weak interstellar features, which are important for accurate abundance measurements. By detecting faint objects well beyond the reach of the *IUE* satellite, the GHRS enables observers to probe gas through the entire halo of the Milky Way, to study conditions in dense interstellar regions with large extinctions, and to obtain absorption-line data for extragalactic systems.

Spectra obtained with the GHRS have stable and well-defined line spread functions, particularly when the small entrance aperture is used. The scattered light in the spectrograph is extremely small ($\ll 1\%$) in the first-order grating modes and is larger (≈ 3–10%) but accurately characterized in the echelle modes (Cardelli et al 1993a). The GHRS wavelength calibration is achieved by viewing a Pt lamp through the entire optical path of the spectrograph. Pt calibration spectra obtained at the same grating carrousel position as the observations result in a wavelength calibration accurate to ≈ 0.3 resolution element (or ≈ 5 and 1 km s^{-1} at intermediate and high resolution, respectively). Without the special calibration exposures, the wavelength calibration is approximately three times less accurate but can sometimes be improved through reference to terrestrial absorption lines. Although the windows and photocathodes of the Digicon detectors introduce fixed-pattern noise, this noise can be removed by obtaining multiple spectra with different detector alignments and solving for the noise pattern in the resulting data (Fitzpatrick & Spitzer 1994; Cardelli & Ebbets 1994). Through this process, Meyer et al (1994) and Lambert et al (1994) have obtained spectra with signal-to-noise ratios approaching 1200.

Figure 1 provides an example of GHRS high-resolution data from Spitzer & Fitzpatrick (1993) that illustrates the spectroscopic richness of the UV wavelength region covered by the GHRS. Interstellar absorption-line profiles are shown for the bright 09.5 Vp star HD 93521, which is situated in the halo 1.5 kpc from the Galactic plane. The complex multicomponent nature of the gas absorption makes it possible to measure the abundances and physical conditions in nine different absorbing structures situated in the Galactic disk and low halo.

4. TECHNIQUES

To obtain accurate column densities, either weak, unsaturated absorption lines or lines so strong they have developed radiation damping wings should be observed. In the weak-line limit, the line is said to lie on the linear portion of the curve of growth. The column density N and equivalent width of the line

W_λ are related through the following equations from Spitzer (1978):

$$W_\lambda = \int [1 - e^{-\tau(\lambda)}] d\lambda; \tag{1}$$

$$\tau(\lambda) = \frac{\pi e^2}{m_e c^2} f \lambda^2 N(\lambda); \tag{2}$$

$$N(\mathrm{cm}^{-2}) = 1.13 \times 10^{17} \frac{W_\lambda(\mathrm{m\AA})}{f \lambda^2(\mathrm{\AA})} \qquad (\tau(\lambda) \ll 1), \tag{3}$$

where λ is the rest wavelength of the line and f is its oscillator strength. In Equation 1, W_λ measures the amount of energy removed by the absorption and is independent of the instrumental resolution. When a line has well-developed damping wings, the following equation may be used to relate W_λ and N on the square root portion of the curve of growth:

$$N(\mathrm{cm}^{-2}) = \frac{m_e c^3}{e^2 \lambda^4} \frac{W_\lambda^2}{f \gamma} = 1.07 \times 10^{33} \frac{W_\lambda^2(\mathrm{m\AA})}{f \gamma \lambda^4(\mathrm{\AA})} \qquad (\tau(\lambda) \gg 1), \tag{4}$$

where γ is the radiation damping constant. In practice, N is generally estimated in this regime through a continuum reconstruction (Bohlin 1975; Diplas & Savage 1994) since the width of the line is usually much larger than the width of the instrumental spread function (i.e. the line is resolved). The H I Lyα line at 1215.67 Å is the most common example of a damped line in the GHRS wavelength range, but in a few cases some strong metal lines (e.g. Mg II $\lambda\lambda$2796, 2803) may also have damping wings (Sofia et al 1994).

The vast majority of interstellar lines normally observed in the GHRS wavelength range have values of $\tau(\lambda)$ that fall somewhere between the two limiting cases of equations 3 and 4. Column density estimates are commonly obtained from lines of intermediate strength through either (*a*) a curve-of-growth analysis in which the total equivalent widths of several lines of the same species are observed and their distribution in the $\log W_\lambda/\lambda - \log N f \lambda$ plane compared with a theoretical curve of growth for a single component subject to a Maxwellian velocity distribution in order to produce a value of N and a Doppler spread parameter b or (*b*) a simultaneous fitting of multiple absorption components having central velocities, widths, and column densities obtained by minimizing the intensity residuals between the observed and predicted absorption profiles for several lines of a species. Rather than describe these methods in detail, we refer the reader to Spitzer (1978). The common pitfalls frequently encountered in abundance studies have been described by Cowie & Songaila (1986) and Jenkins (1987). These problems include (but are not limited to) improper use of the standard curve of growth for strongly saturated lines, invalid application

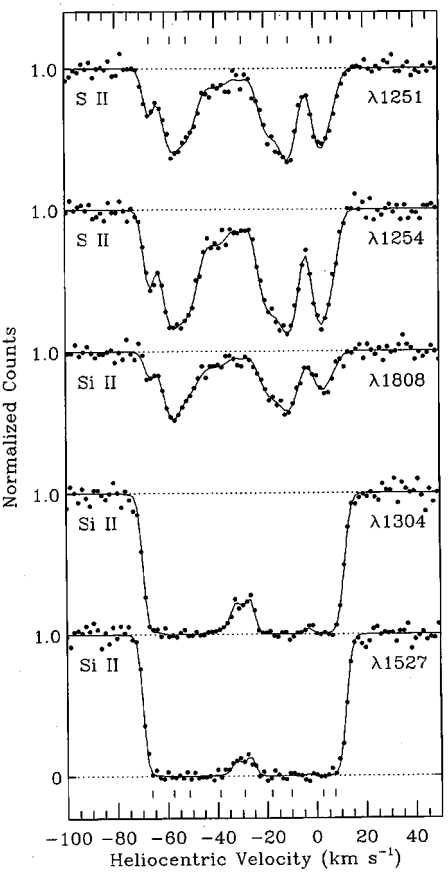

Figure 1 Normalized intensity vs heliocentric velocity for a suite of interstellar lines toward the halo star HD 93521. These GHRS high-resolution data (shown as solid points) reveal a rich velocity structure spanning nearly 90 km s^{-1}. Data of this quality make possible study of the abundances and physical conditions in individual clouds in the ISM along the sight line. The absorption lines shown cover a large range of line strengths, from relatively weak lines (Mg II λ1240 and Mn II λ2606) to very strong lines (Fe II λ2600 and Si II λ1526). Tick marks at the top and bottom of each panel indicate the velocities of the absorption components used to construct the theoretical profiles drawn with solid lines (from Spitzer & Fitzpatrick 1993).

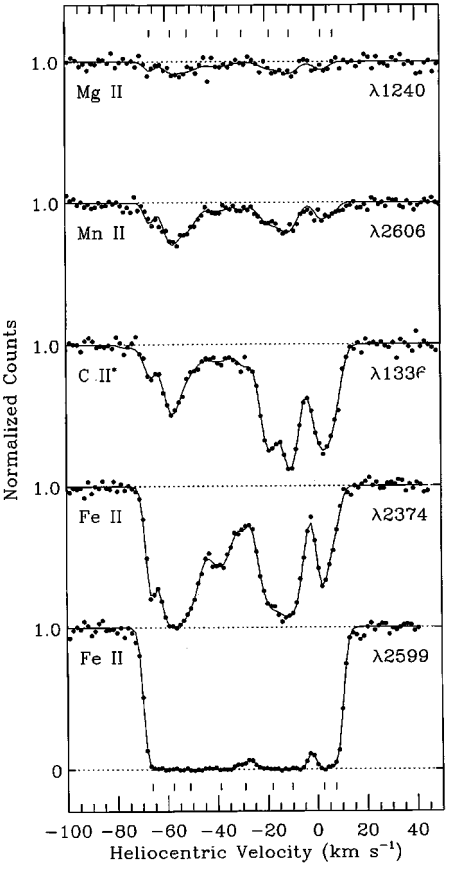

Figure 1 (*Continued*)

of curves of growth across species, inability to distinguish H I from H II region contributions, improper or insufficient treatment of errors, and uncertainties in f-values and cosmic reference abundances. Throughout this paper we reiterate some of these potential problems in the context of higher-resolution data available with the GHRS.

When the instrumental resolution is sufficiently high that an absorption profile (or portion thereof) is close to being resolved or the optical depth of the absorption is small, some of the problems caused by the assumption of a velocity distribution for the absorbing clouds can be circumvented by examining the profiles in terms of their apparent column density profiles (see Savage &

Sembach 1991). The apparent optical depth for the intensity of an observed line at a velocity v is given by

$$\tau_a(v) = -\ln[I_{obs}(v)/I_o(v)] = -\ln[e^{-\tau(v)} \otimes \phi_I(v)], \quad (5)$$

where I_o is the continuum intensity in the absence of absorption and $\phi_I(v)$ is the instrumental spread function. The apparent column density $N_a(v)$ is related to $\tau_a(v)$ through an equation similar to Equation 2:

$$N_a(v) = \frac{m_e c}{\pi e^2} \frac{\tau_a(v)}{f\lambda}$$

$$= 3.768 \times 10^{14} \frac{\tau_a(v)}{f\lambda(\text{Å})} \text{ [atoms cm}^{-2}\text{(km s}^{-1})^{-1}\text{]}. \quad (6)$$

$N_a(v)$ is an apparent column density per unit velocity because its value depends on the resolution of the spectrograph and on the apparent shape of the line. The total apparent column density is $N_a = \int N_a(v)dv$. In the limit where the absorption line is weak ($\tau \ll 1$) or fully resolved [FWHM (line) > FWHM (ϕ_I)], the total apparent column density, N_a, and the true column density, N, are equal.

Many interstellar lines arising in H I regions are not fully resolved even at the highest resolution of the GHRS. In such cases, a comparison of the $N_a(v)$ profiles for two or more lines having different values of $f\lambda$ provides information about the amount and velocity of unresolved saturated structure within the lines. When unresolved saturated structure exists in the lines, the $N_a(v)$ profile of a stronger line underestimates the $N_a(v)$ profile of the weaker line at those velocities, and $N_a(v) < N(v)$. Those portions of the $N_a(v)$ profiles that agree provide valid instrumentally smeared versions of $N(v)$ and, in principle, of $N_a = N$ over those velocity ranges. For doublet lines having values of N_a agreeing to within 20%, the difference between the true column density and the value of N_a for the weaker member of the doublet is equal to the difference in the values of N_a for the doublet (i.e. $N = N_a + \Delta N_a$). Savage & Sembach (1991) have considered the analysis of apparent column density profiles for doublet lines and describe the use of this method in detail.

The main advantage of using the apparent column density method over traditional curve-of-growth techniques for analyses of intermediate-strength absorption lines is the conversion of the data into a form directly suitable for species-to-species comparisons as a function of velocity. No requisite assumption is made about the velocity distribution of the gas since the velocity information is retained in the analysis.

5. OSCILLATOR STRENGTHS

The accuracy of atomic oscillator strengths often limits the accuracy of interstellar abundance measurements. In a compilation important for interstellar studies, Morton (1991) surveyed the available atomic data and recommended a set of oscillator strengths for absorption lines with $\lambda > 912$ Å for a large number of abundant elements through $Z = 32$. Many observers use these oscillator strengths. In this section, we list some of the improvements made since Morton's compilation and extend the list to include some of the rarer elements not found in his tabulation.

Several other recent compilations of oscillator strengths have been performed. Fuhr & Wiese (1991) critically evaluated oscillator strengths for 63 elements through $Z = 83$ (bismuth). Their compilation includes 8300 spectral lines arising from various atomic levels. Verner et al (1994) assembled a list of absorption-line f-values from the ground level of atoms through $Z = 83$ for $\lambda > 228$ Å. Their work merges the compilation of Morton (1991) and that of Fuhr & Wiese (1991) with recent theoretical calculations from the Opacity Project (OP) (Seaton et al 1992), which has produced a complete set of accurate atomic data for permitted transitions involving all stages of ionization of abundant elements with $Z = 1$–14, 16, 18, 20, and 26. A comparison of these theoretical oscillator strengths with experimental results confirms the general reliability of the OP data (Seaton et al 1992; Mendoza 1992; Verner et al 1994). However, the OP f-value calculations assume good LS coupling, and in specific cases, configuration interaction can introduce large systematic errors.

Wavelengths and oscillator strengths for very heavy elements ($Z > 32$) with lines in the GHRS wavelength range likely detectable in absorption in diffuse clouds with $N(\mathrm{H}) > 10^{21}$ cm^{-2} can be found in Cardelli et al (1993b). Their list does not include absorption lines for which the expected line strength is less than ≈ 0.1 mÅ. Such a limit is probably reasonable since to date the weakest ISM lines detected with $> 3\sigma$ significance in very high signal-to-noise (S/N) spectra obtained with the GHRS have equivalent widths of $\approx 0.3 - 0.5$ mÅ (Cardelli et al 1993c; Federman et al 1995). Note that the Ge II λ1237.06 f-value listed in Morton (1991) and carried over to Verner et al (1994) contains a decimal error. The correct value should be 0.876. Since the compilation of Cardelli et al (1993b), Brage & Leckrone (1995) have reported new f-values for As II.

In Table 2 we list new or revised f-values important in determining abundances for dominant ions of abundant elements in interstellar H I regions. The footnotes to the table indicate the sources of the f-values; some are from new experimental measurements, others are from theory, and a few are based on GHRS ISM data.

An important effort in the pursuit of accurate oscillator strengths for ISM studies is the experimental program of Bergeson & Lawler (Refs. 2, 5, and 7 in Table 2), in which laser-induced fluorescence lifetime measurements of selectively excited upper levels are used to determine accurate transition lifetimes. These data, together with reliable branching ratios (when necessary), have yielded f-values with $\approx 10\%$ accuracy for Si II λ1808, Cr II $\lambda\lambda$2056, 2062, 2066; Zn II $\lambda\lambda$2026, 2062; and Fe II λ2249, 2260. These lines often are observed in abundance studies of gas in the Milky Way and in galaxies in the distant Universe.

Interstellar studies with the GHRS also have led to improved values of some atomic and molecular oscillator strengths. For example, new empirical oscillator strengths have been determined for lines of Si II (Spitzer & Fitzpatrick

Table 2 Oscillator strength update[a]

Ion	λ(vacuum) Å	f(Morton)	f(Revised)	Technique[b]	Source[c]
C II.....	2325.403	4.48×10^{-8}	5.80×10^{-8}	E	1
Mg II.....	1240.3947	1.34×10^{-4}	6.25×10^{-4}	I	4
	1239.9253	2.68×10^{-4}	1.25×10^{-3}	I	4
Si II.....	2335.123	3.72×10^{-6}	4.25×10^{-6}	E	8
	1808.0126	5.53×10^{-3}	2.18×10^{-3}	E,T	2,11
	1304.3702	1.47×10^{-1}	8.60×10^{-2}	I,T	3,11
	1526.7006	2.30×10^{-1}	1.10×10^{-1}	I,T	3,11
Cl I.....	1088.0589	1.59×10^{-2}	8.10×10^{-3}	E	9
	1097.3692	4.23×10^{-2}	8.80×10^{-3}	E	9
	1347.2396	1.19×10^{-1}	1.53×10^{-1}	E	9
	1363.4476	9.77×10^{-2}	5.50×10^{-2}	E	9
Ar I.....	1048.2199	2.44×10^{-1}	2.57×10^{-1}	E	10
	1066.6599	6.65×10^{-2}	6.40×10^{-2}	T	10
Cr II.....	2056.254	1.40×10^{-1}	1.05×10^{-1}	E	5
	2062.234	1.05×10^{-1}	7.80×10^{-2}	E	5
	2066.161	6.98×10^{-2}	5.15×10^{-2}	E	5
Fe II.....	1608.4511	6.19×10^{-2}	6.19×10^{-2}	I,E	6,13
	1611.2005	2.22×10^{-4}	1.02×10^{-3}	I	6
	2249.8768	2.51×10^{-3}	1.82×10^{-3}	E	7,12
	2260.7805	3.72×10^{-3}	2.44×10^{-3}	E	7,12
	2374.4612	2.82×10^{-2}	3.26×10^{-2}	I,E	6,12
	2586.6500	6.46×10^{-2}	6.84×10^{-2}	I,E	6,12
Zn II.....	2026.136	5.15×10^{-1}	4.89×10^{-1}	E	5
	2062.664	2.53×10^{-1}	2.56×10^{-1}	E	5

[a]We list important improvements to oscillator strengths made since the compilation of Morton (1991) for dominant ion lines of abundant elements found in H I regions. Results from the extensive Opacity Project (OP) data base (Seaton et al 1992) are not listed since they have been compiled by Verner et al (1994). In some cases, OP f-values are superior to other experimental or theoretical values.

[b]The technique used to obtain the listed f-value is indicated. E and T indicate experimental and theoretical f-values, respectively. I indicates that the f-value is based on an interstellar absorption-line analysis method.

[c]The new f-values are from the following references: (1) Fang et al (1993) and branching ratios from Lennon et al (1985); (2) Bergeson & Lawler (1993b); (3) Spitzer & Fitzpatrick (1993); (4) Sofia et al (1994); (5) Bergeson & Lawler (1993a); (6) Cardelli & Savage (1995); (7) Bergeson et al (1994); (8) Calamai et al (1993); (9) Schectman et al (1993); (10) Federman et al (1992); (11) Dufton et al (1983, 1992); (12) Bergeson et al. (1996a); (13) Bergeson et al. (1996b).

1993), S I (Federman & Cardelli 1995), and Fe II (Cardelli & Savage 1995). Sofia et al (1994) compared column densities for C, N, O, and Mg derived from very strong (damped) lines and from weak lines with little saturated structure. In all cases, the strong-line f-values were well-known, thus permitting a check on the accuracy of the weak-line f-values. For O I (λ1302.2 vs λ1355.6), C II (λ1334.5 vs λ2325.4), and N I (λ1200.7 vs λ1160.9), the strong and weak lines yielded consistent column densities within the experimental errors of $\approx\pm$ 0.1 dex. However, for Mg II (λ2803.5 vs $\lambda\lambda$1239.9, 1240.4), the strong lines gave a Mg II column density 4.7 times smaller than did the weak lines when using the Morton (1991) f-values. The new empirical f-values for Mg II $\lambda\lambda$1239.9, 1240.4 listed in Table 2 reflect this difference. Given the importance of Mg in astrophysical environments, these new f-values should be verified experimentally.

Morton & Noreau (1994) present an extensive compilation of wavelengths and oscillator strengths for 1500 electronic transitions of CO between 1000 and 1545 Å. A comparison of their results with the existing CO interstellar absorption-line literature provides consistency checks on f-values and information about CO line saturation corrections. Several of the small f-value transitions revealed through this investigation will be useful in studying the amount of CO in high-column density clouds.

6. THE GHRS ISM ABSORPTION-LINE DATA BASE

Many GHRS interstellar absorption-line observations have come from programs specifically designed for ISM science, whereas others have been by-products of the in-orbit scientific verification of the spectrograph. Table 1 contains a listing of ions observed with the GHRS. Many, but not all, of these ions have been detected in the interstellar clouds toward ζ Oph. Table 3 provides a summary of some of the sight lines for which extensive interstellar GHRS observations have been published. The list includes sight lines for which at least five elements have been studied and does not include objects such as β Pictoris, for which the absorption is primarily circumstellar. For each object the table lists the Galactic coordinates, distance, B-V color excess, total hydrogen column density $\equiv [N(\mathrm{H\ I}) + 2N(\mathrm{H_2})]$, GHRS resolution mode (H = high; I = intermediate), elements studied, and primary references.

Few high-resolution observations have been made for objects fainter than $V \approx 9$, but substantial intermediate-resolution data are available. The 3C 273 sight line is the most extensively studied extragalactic direction at the intermediate resolution of the GHRS. Archival research has provided information about individual interstellar species along many sight lines (Cardelli 1994; Roth & Blades 1995; Sembach et al 1995b).

Table 3 The GHRS ISM absorption line database (studies of $\geq$ 5 elements)[a]

HD	Name	l (deg)	b (deg)	d (pc)	E(B-V) (mag)	log N(H) (cm^{-2})	Mode[b]	Elements studied	Ref.[d]
18100	.....	217.9	-62.7	3100	0.02	20.14	I/H	Mg, Si, S, Mn, Cr, Fe	1
22586	.....	264.2	-50.4	2000	0.06	20.35	I	O, Mg, Al, Si, S, Fe, Ni	2
24912	ξ Per	160.4	-13.1	540	0.32	21.29	I/H	Many elements - see Table 5	3
35149	23 Ori	199.2	-17.9	430	0.11	20.74	I	Cu, Ga, Ge, Kr, Sn	4
38666	μ Col	237.3	-27.1	1070	0.02	19.85	H	C, O, Mg, Al, Si, S, Cr, Mn, Fe, Ni, Zn	5
47839	15 Mon	202.9	+2.2	700	0.07	20.40	I	Cu, Ga, Ge, Kr, Sn	6
49798	.....	253.7	-19.1	650	0.02	...	I	O, Mg, Al, Si, S, Fe	7
68273	γ^2 Vel	262.8	-7.7	450	0.04	19.74	H	C, Mg, Si, P, S, Mn, Fe	8
72089	.....	263.2	-3.9	1700	...	...	I	O, Mg, Al, Si, S, Fe, Ni	9,11
72127[c]	.....	262.6	−3.4	600	0.08	...	I	C, O, Mg, Si, P, S, Ge	10
93521	.....	183.1	+62.2	1700	0.02	20.10	H	C, Mg, Si, S, Mn, Fe	12
116852	.....	304.9	-16.1	4800	0.22	20.96	I/H	Mg, Si, P, S, Mn, Cr, Fe, Ni, Zn, Ge	13
120086	.....	329.6	+57.5	1000	0.04	20.41	I	O, Mg, Al, Si, S, Fe, Ni	14
141637	1 Sco	346.1	+21.7	170	0.20	21.20	I	Cu, Ga, Ge, Kr, Sn, Pb	15
143018	π Sco	347.2	+20.2	170	0.08	20.75	I	Cu, Ga, Ge, Kr, Sn	16
149757	ζ Oph	6.3	+23.6	140	0.32	21.13	I/H	Many elements - see Table 5	17
149881	.....	31.4	+36.2	2100	0.07	20.57	H	Mg, Si, S, Cr, Mn, Fe	18
154368	.....	350.0	+3.2	800	0.82	21.62	I/H	C, O, Mg, Al, Si, P, S, Mn, Ni, Zn	22
167756	.....	351.5	-12.3	4000	0.09	20.81	H	Mg, Si, Cr, Fe, Zn	19
212571	π Aqr	66.0	-44.7	315	0.23	20.56	I	Cu, Ga, Ge, Kr, Sn	20
.....	3C 273	290.0	+64.4	.....	.....	20.10	I	Mg, Si, S, Mn, Fe, Ni	21

[a]Sight lines for which extensive ISM data have been obtained and reported in the literature. For many sight lines not listed here, fewer than five interstellar species have been detected and studied in detail.
[b]I and H refer to the GHRS intermediate- and high-resolution modes, respectively.
[c]Binary system with a separation of 4.5". Absorption toward both stars has been studied.
[d]References: (1) Savage & Sembach (1994), Sembach & Savage (1996); (2) Jenkins & Wallerstein (1996); (3) Cardelli et al (1991b), Savage et al (1991), Smith et al (1991), Lambert et al (1995); (4) Hobbs et al (1993); (5) Sofia et al (1993); (6) Hobbs et al (1993); (7) Jenkins & Wallerstein (1996); (8) Fitzpatrick & Spitzer (1994); (9) Jenkins & Wallerstein (1995); (10) Wallerstein et al (1995a); (11) Jenkins & Wallerstein (1996); (12) Spitzer & Fitzpatrick (1992, 1993); (13) Sembach & Savage (1994, 1996); (14) Jenkins & Wallerstein (1996); (15) Hobbs et al (1993), Welty et al (1995); (16) Hobbs et al (1993), Lambert et al (1995); (17) Cardelli et al (1991a, 1993b, 1993c, 1994), Savage et at (1992), Federman et al (1993, 1994), Hobbs et al (1993), Cardelli (1994), Lambert et al (1994, 1995), Lyu et al (1994), Sembach et al (1994), Tripp et al (1994); (18) Spitzer & Fitzpatrick (1995); (19) Savage et al (1994), Cardelli et al (1995); (20) Hobbs et al (1993); (21) Savage et al (1993b); (22) Snow et al (1996).

7. NOTATION AND TERMINOLOGY

We have adopted a system of notation similar to that used in the stellar abundance literature. N(X) refers to the total column density (atoms cm^{-2}) of species X in a H I region. Generally, N(X) is closely approximated by either N(X I) or N(X II), depending whether the ionization potential of the neutral atom is greater or less than 13.6 eV. For hydrogen, $N(H) = N(H\ I) + 2N(H_2)$, where $N(H_2) = \Sigma N(H_2)_J \approx N(H_2)_0 + N(H_2)_1$. Most of the molecular hydrogen is in the two lowest rotational levels ($J = 0$ and 1) in interstellar clouds in which $n(H_2)/n$(H I) is more than $\approx 1\%$ (Savage et al 1977). Therefore, the gas-phase abundance

of species X with respect to hydrogen is $(X/H)_g = N(X)/N(H)$, where g refers to gas. The normalized gas-phase abundance with respect to cosmic abundances is $(X/H)_g/(X/H)_c$, where c refers to cosmic. We adopt the standard logarithmic notation system used in stellar astrophysics: $[X/H] \equiv \log (X/H)_g - \log(X/H)_c$.

In the ISM literature, the linear depletion $\delta(X)$ of species X is defined as $\delta(X) = (X/H)_g/(X/H)_c$, and the logarithmic depletion is $D(X) = [X/H]$. The linear and logarithmic depletions are simply the linear and logarithmic gas-phase abundances of a species referenced to cosmic or solar abundances. If $\delta(X) = 1.0$ or $D(X) = 0.00$, then element X has an interstellar gas-phase abundance equal to its cosmic abundance. An element is said to be depleted if $\delta(X) < 1.0$. For lightly depleted elements, $0.3 < \delta(X) < 1.0$, whereas highly depleted elements have $\delta(X)$ as small as 0.001. Highly depleted elements have large depletion factors, where the term depletion factor is defined as $1/\delta(X)$. One generally assumes that the amount of a given species missing from the gas is contained in the interstellar dust. Therefore, we also define a linear dust-phase abundance $(X/H)_d = (X/H)_c - (X/H)_g$ and a corresponding logarithmic dust-phase abundance $\log(X/H)_d = \log\{(X/H)_c - (X/H)_g\}$. For a highly depleted element [small $(X/H)_g$], the dust-phase abundance is essentially equal to the cosmic abundance $(X/H)_c$.

8. COSMIC REFERENCE ABUNDANCES

To understand the significance of interstellar gas-phase abundance measurements, we need measures that represent the total (gas + dust) abundances for young Population I matter. However, the required set of abundances does not exist, so solar system abundances commonly are adopted as the cosmic references. However, several other reference standards also could be used. Table 4 lists recent abundance measurements for H II regions, main-sequence B stars, and the Sun.

Temperature fluctuations in H II regions affect the abundances derived from collisionally excited emission lines (for reviews see Peimbert 1995 and Mathis 1995). The H II region abundances in Table 4 are averages for M8, M17, and Orion (Peimbert et al 1993) based on the assumption that strong temperature fluctuations occur within the nebulae, producing collisionally excited lines in hotter regions and recombination lines in cooler regions. The gas abundances derived from collisionally excited emission lines in the absence of temperature fluctuations are typically 0.25 dex lower than the values given in Table 4 (see Table 7 of Peimbert et al 1993). The most compelling argument for large temperature fluctuations in H II regions is that the abundances derived from collisionally excited emission lines and recombination lines for C and O can be brought into agreement (Peimbert 1995). However, Mathis (1995) concludes

that nebular abundance measurements may contain large systematic errors, and he believes that present-day published nebular abundances are suspect even if they include the effects of temperature fluctuations. Similar concerns have been expressed by Kingdon & Ferland (1995), who have calculated nebular models including the effects of temperature fluctuations. As we discuss in Section 12, absorption-line measures of the interstellar oxygen abundance are difficult to interpret if either the H II region abundances or the solar abundances listed in Table 4 are the appropriate reference abundances of ISM studies.

The B-star abundances listed in Table 4 come from two sources: Gies & Lambert (1992) and Figure 2 of Kilian-Montenbruck et al (1994). Both studies focus primarily on main-sequence B stars in the solar neighborhood, and results are from both line-blanketed LTE model atmospheres and NLTE model atmospheres. These separate B-star results compare favorably for C, N, and O (difference < 0.15 dex), but there are large differences (> 0.2 dex) for Ne, Al, Si, S, and Fe. The B-star abundances listed in Table 4 generally span the range of values found for independent LTE model atmosphere calculations for B stars in the solar neighborhood (Fitzsimmons et al 1990) and for B stars in clusters within 4–5 kpc of the Sun (Rolleston et al 1993, 1994). However, inhomogeneities in the ISM may result in significantly different abundances for

Table 4 Reference abundance comparison

X	$\log(X/H)^a_{H\ II}$	$\log(X/H)^b_{B\ star}$		$\log(X/H)^c_\odot$	$\Delta(\langle B\ star\rangle - Sun)^d$
		GL	KM		
C	-3.40	-3.80	-3.73	-3.45	-0.31
N	-4.11	-4.19	-4.20	-4.03	-0.17
O	-3.23	-3.32	-3.44	-3.13	-0.25
Ne	-3.97	-4.03	-3.80	-3.91	-0.01:
Mg	...	...	-4.62	-4.42	-0.20
Al	...	-5.55	-5.81	-5.52	-0.16:
Si	...	-4.42	-4.80	-4.45	-0.16:
S	-4.69	-4.79	-5.03	-4.73	-0.18:
Fe	-5.41	-4.28	-4.60	-4.49	+0.05:

[a]H II region reference abundances are averages of values for M8, M17, and the Orion Nebula (Peimbert et al 1993) and assume substantial nebular temperature fluctuations. If there are no temperature variations, the reported H II region abundances decrease by typically 0.25 dex. For Fe, and possibly for C and O, the listed H II region gas-phase abundances may be smaller than the total abundance (gas + dust) if these elements are constituents of nebular dust.

[b]B-star reference abundances listed in the column labeled GL are from Gies & Lambert (1992), and those listed in the column labeled KM are from a least-squares fit to the measurements in Figure 2 of Kilian-Montenbruck et al (1994) for $R_g = 8.5$ kpc. Note the substantial disagreement between GL and KM (> 0.2 dex) for Ne, Al, Si, S, and Fe.

[c]Solar reference abundances are the meteoritic abundances given by Anders & Grevesse (1989) except for C, N, and O, which are the solar photospheric values from Grevesse & Noels (1993), who allow for the effect of recent revisions of the Fe abundance on gas and electron pressures in solar model atmospheres.

[d]We list the logarithmic differences between the average B-star abundance and the solar abundance. When the B-star abundances disagree by more than 0.20 dex, we attach a colon to the value.

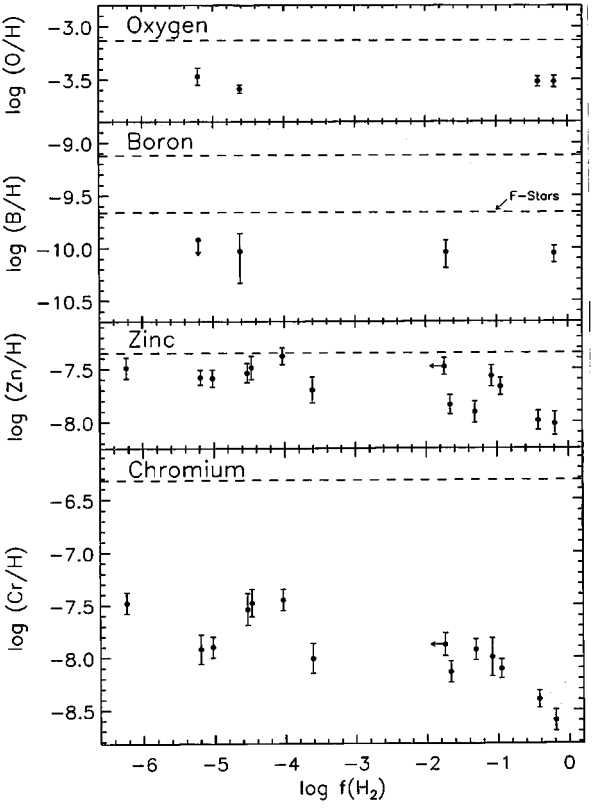

Figure 2 GHRS measurements of the logarithmic abundance of O, B, Zn, and Cr relative to H vs molecular hydrogen fraction $f(H_2) = 2N(H_2)/[N(H\,I) + 2N(H_2)]$. The dashed line immediately below the element name in each panel is the value of log(X/H) for the solar system (see Table 1). For boron, the lower dashed line indicates the reference abundance favored by Federman et al (1993). The two points having the highest molecular hydrogen fraction are ξ Per and ζ Oph. Data for this figure come from the following studies and references cited therein: O (Meyer et al 1994), B (Jura et al 1996) Zn and Cr (Roth & Blades 1995, Sembach et al 1995b).

individual clusters separated by less than a few kiloparsecs (see Lennon et al 1990; Rolleston et al 1994).

The solar abundances listed in Table 4 are the meteoritic abundances given by Anders & Grevesse (1989), with the exception of C, N, and O, which are the solar photospheric values from Grevesse & Noels (1993). These studies yield meteoritic and photospheric abundances that generally agree to within ≈ 0.04 dex and show that several long-standing discrepancies for key elements such as Fe have been resolved.

The last column of Table 4 lists the logarithmic differences between an average of the two B-star abundances and the solar abundances. When the two B-star abundance values differ by ≥ 0.20 dex, we attach a colon to the value of $\Delta(\langle\text{B star}\rangle - \text{Sun})$. With the exception of Ne and Fe, the average B-star abundances are lower than the solar abundances by approximately 0.2 dex. For C, N, and O, the differences range from -0.31 to -0.17 dex. A 4.6-Gyr star may have higher heavy-element abundances than the youngest stars in the solar neighborhood because of incomplete mixing of the Galactic gas, which results in abundance inhomogeneities (Gies & Lambert 1992). Alternatively, the local region of the Galaxy may have experienced a recent inflow of metal-poor material (Meyer et al 1994; Jura et al 1996).

In principle, X-ray astronomy could provide a reliable oxygen reference abundance. Schattenburg & Canizares (1986) reported an interstellar value of $N(\text{O}) = (2.78 \pm 0.55) \times 10^{18}$ cm^{-2} toward the Crab Nebula based on the detection of the oxygen K-shell edge. Because K-shell absorption records the presence of O in both the gas and solid phases, the value should reflect the total line-of-sight oxygen column density. These authors found that $\log(\text{O/H}) = -3.08^{+0.11}_{-0.14}$, which is in agreement with the solar value. Unfortunately, because the total hydrogen column density toward the Crab Nebula is uncertain, this oxygen abundance may be subject to additional systematic errors.

Given the above considerations, we reference the ISM gas-phase abundances to the solar abundances listed in Table 1. We also discuss the effects of a 0.20-dex lowering of the abundances of all elements compared with the solar abundances in order to explore changes in the results if B-star abundances are used. This approach seems to be more practical than choosing a whole suite of new reference abundances for each of the many elements measured in B stars and in H II regions.

9. IONIZATION EFFECTS

For most elements, the singly ionized stage is dominant in the neutral ISM because the first ionization potential is below 13.6 eV and the second is above the H ionization threshold (see Table 1). Notable exceptions to this rule are N, O, Ar, and Kr, which have first ionization potentials ≥ 13.6 eV, and Ca II, which has a second ionization potential < 13.6 eV. Moreover, for some elements (e.g. Mg, Al, and Cl), dielectronic recombination or ion-molecule reactions may alter the balance of ion stages, depending on the conditions of the environment encountered (Jura 1974; York & Kinahan 1979).

In abundance studies of interstellar clouds, the total amount of an element is usually assumed to be equal to the amount present in the primary stage of ionization in H I regions. This assumption can lead to substantial abundance

errors if a mix of H I and H II region gas is present along the sight line or within the cloud under study. One possible means to correct for the relative contributions of the two types of regions is to assume an equilibrium situation in which recombinations balance photonionization. The ratio of gas densities in adjoining ionization stages is then given by the familiar equation:

$$n(X^{i+1})/n(X^i) = \Gamma(X^i)/[n_e\alpha(T, X^{i+1})]. \quad (7)$$

If collisional ionization processes are not significant, the ionic ratio in this simplest case depends on the electron density n_e; on the photoionization rate $\Gamma(X^i)$, which converts X^i into X^{i+1}; and on the temperature through the recombination coefficient $\alpha(T)$, which may contain both a radiative and a dielectronic component. Additional terms describing charge-exchange reactions between neutral and singly ionized atoms are not included in Equation 7 but may be important for the production or destruction of some species in H I regions and should not be ignored. Péquignot & Aldrovandi (1986) list H I region charge-exchange rates for various ion-neutral pairs as well as updated estimates for radiative recombination coefficients (Aldrovandi & Péquignot 1973; Gould 1978; see also Péquignot et al 1991). Photoionization rates are given by de Boer et al (1973), Witt & Johnson (1973), Gondhalekar & Wilson (1975), and Draine (1978; see also Reilman & Manson 1979). Dielectronic recombination coefficients for many ions can be found in Aldrovandi & Péquignot (1973, 1974, 1976) and Nussbaumer & Storey (1983, 1984, 1986).

Knowledge of several of the quantities in Equation 7 and measurements of $N(X^i)$ and/or $N(X^{i+1})$ yield information about the remaining unknown quantities. The volume densities in Equation 7 are usually replaced by column densities, i.e. $n(X^i)/n(X^{i+1}) \approx N(X^i)/N(X^{i+1})$, although this substitution may not be valid in some cases and is best verified through high-resolution observations, which reveal the velocity structure of the absorption lines or apparent column density profiles.

Equation 7 also provides a means for determining H I region abundances when only trace ionization states of elements are observed. For example, Morton (1975) applied this technique successfully to derive abundance measurements for Li, Na, K, and Ca from optical measurements of the trace ions Li I, Na I, K I, and Ca II by using *Copernicus* satellite observations of dominant ion lines of other elements in the UV to determine n_e and T in the cool diffuse interstellar cloud toward ζ Oph. More recently, Federman et al (1993) used GHRS measurements of the weak S I lines and ionization balance to determine a S abundance for the cloud since the S II lines are strongly saturated.

Because temperatures and densities determined from dominant ion lines may differ from those appropriate for regions forming the trace ion lines, abundance estimates that rely on trace ions and on the assumption of ionization equilibrium

often incur additional uncertainties. Relative depletion and ionization effects between trace and dominant ions may affect the results, as compositional differences and physical conditions change within individual clouds or from one cloud to the next since the local density scales as $n_{\rm H}^2$ for trace ions and as $n_{\rm H}$ for dominant ions (Jenkins 1987). Preferential incorporation of refractory elements into dust grains (see Sections 10, 12–13) and their subsequent release back into the gas phase under different conditions make comparisons of these elements with volatile elements particularly troublesome.

The assumption of ionization balance appears valid for the diffuse neutral interstellar cloud (the Local Cloud) surrounding the Sun. GHRS measurements of Mg I and Mg II absorption toward Sirius yield an electron density $n_{\rm e} = 0.19$–0.39 cm^{-3} and a temperature $T = 7600 \pm 3000$ K under the assumption of ionization balance defined in Equation 7 (Lallement et al 1994). These results are compatible with the electron density $n_{\rm e} = 0.22$–0.44 cm^{-3} required to explain the carbon component of the anomalous cosmic ray population in the Solar System (Frisch 1994) and with the temperatures $T = 7000 \pm 200$ K and $T = 6700 \pm 200$ K determined from GHRS line width measurements of D I and H I in the local ISM toward Capella and Procyon (Linsky et al 1993, 1995). The value of $\Gamma({\rm Mg\ I}) = 4.0 \times 10^{-11}$ s^{-1} (Frisch et al 1990) is rather well-known for the solar neighborhood since the 1200–1620-Å photons that create Mg II pass freely into and through H I regions.

Extreme Ultraviolet Explorer Satellite (EUVE) measurements of EUV (504–703 Å) radiation from ε CMa (Cassinelli et al 1995) imply that the star dominates the local stellar EUV radiation field. The measurements set a lower limit of 10–20% for the hydrogen ionization fraction in the local ISM due to stellar sources (Vallerga & Welsh 1995). An ionization fraction close to 15% for the very local ISM is compatible with the higher value of $\sim 50\%$ found for the heliosphere if charge-exchange processes operate at the heliopause (Ripken & Fahr 1983; see also Clarke et al 1995). The *EUVE* result implies an ionization fraction for the local ISM of 70–80% for $n({\rm H^o}) = 0.1$ cm^{-3} (Frisch 1994) unless the interstellar cloud surrounding the Sun is subject to ionizing sources other than local hot stars, such as residual radiation from a recent ($t < 300{,}000$ years) supernova or from a conductive interface between the Local Cloud and the surrounding hot ($T \sim 10^6$ K) ISM of the Local Bubble (Slavin 1989; Vallerga & Welsh 1995). Recent GHRS measurements of the C IV and Si III-IV absorption toward ε CMa (Gry et al 1995) support the idea that a thermal conduction front at the boundary of the Local Cloud contributes to the ionization of the local interstellar gas in this direction.

In addition to the assumption of photon ionization balance, other methods can be used to determine temperatures and densities in various interstellar

environments. For example, Jenkins & Wallerstein (1995) used the GHRS to study the C I fine-structure levels in recombining gas behind a shock front in the Vela SNR. The pressure of the gas is sufficiently high to produce observable fine-structure lines of neutral carbon. In this particular instance, the C I fine-structure levels are populated by collisions in proportion to their level degeneracies, resulting in estimates of $1000 < n_{\rm H} < 2900$ cm^{-3} and $300 < T < 1000$ K in the absence of observable O I fine-structure lines. Smith et al (1991) also used the ratios of C I fine-structure lines to determine pressures in several of the diffuse cloud components toward ξ Per. They found a very high pressure for the strongest component at $v_{\rm helio} = +6$ km s^{-1}, $\log(P/k) \geq 4.3$ for $T = 32$ K as well as a pressure which is a factor of ten lower in the component near $v_{\rm helio} = +10$ km s^{-1}. Substantial changes occur in the abundances of atomic species between these two clouds as well (see Section 10). Collisional population of the fine-structure levels of C II and Si II also has been used to study conditions in the neutral and ionized gases in diffuse interstellar disk and halo clouds and in H II regions (e.g.) Spitzer & Fitzpatrick 1993, 1995; Fitzpatrick & Spitzer 1994).

High-resolution GHRS observations have been used successfully to identify narrow absorption components resulting from ionized gas tracers such as Al III, P III, S III, Si IV, and C IV in H II regions toward stars with diffuse H I clouds at nearby velocities (ζ Oph: Sembach et al 1994; γ^2 Vel: Fitzpatrick & Spitzer 1994). However, even if accurate column densities can be obtained for some H II region species, the interaction of stellar winds, depletion onto dust, and insufficient knowledge of the stellar flux distribution below 912 Å can seriously affect conclusions about H II region abundances derived from absorption-line data (see also Section 8). This last problem appears to be particularly acute in light of the recent *EUVE* measurement by Cassinelli et al (1995; see also Vallerga & Welsh 1995), which showed that the local ISM hydrogen ionization parameter $\Gamma({\rm H})_{\rm LISM} = 1.1 \times 10^{-15}$ s^{-1} resulting from ε CMa alone is approximately six to seven times greater than previously estimated for the integrated value from all nearby stars combined (Bruhweiler & Cheng 1988).

H II regions outside the immediate vicinity of hot stars also may affect interstellar abundance determinations. Models of ionic ratios in partially ionized diffuse gases (Dömgorgen & Mathis 1994) are often necessary for studies of the ISM in the low Galactic halo since Hα background measurements suggest that the Milky Way ISM contains a diffuse, ionized gas component with a filling fraction of $\sim$ 20% (Reynolds 1993 and references therein). Useful combinations of ions observable with the GHRS that yield ionization information about interstellar clouds include C I-II-IV, Mg I-II, Al II-III, P I-II-III, Si I-II-III-IV,

and S-II-III. Sembach & Savage (1996) found that corrections of ≈ 0.15–0.20 dex are required in order to convert the abundances derived from standard H I region assumptions to total (H I + H II region) abundances if the diffuse halo clouds toward HD 116852 ($d = 4.8$ kpc; $l = 304.9^\circ$; $b = -16.1^\circ$) are partially ionized by the dilute radiation responsible for the diffuse Hα background.

Photons from O stars in the Galactic disk may be the primary source of ionization of the warm extended ($|z| \sim 1$ kpc) medium in the Milky Way (Miller & Cox 1993; Dömgorgen & Mathis 1994; Dove & Shull 1994). However, Spitzer & Fitzpatrick (1993) noted that the warm neutral and warm ionized gases seem to be well-mixed in the clouds toward the halo star HD 93521. They believe that the partial ionization in these clouds probably cannot be produced by starlight photoionization and suggest a number of alternate ionization processes, including collisional ionization from shocks, X-ray photoionization, and energetic charged-particle ionization.

The integrated flux of extragalactic background radiation from active galactic nuclei may strongly affect the ionization properties of more distant interstellar clouds (Bregman & Harrington 1986). Therefore, studies of abundances in the Magellanic Stream or distant outer Galaxy also must rely on photoionization models (Lu et al 1994a,b). In the distant high-velocity clouds toward Markarian 509, ionization of the interstellar gas is unusual; the clouds are seen in absorption only in C IV, not in NV or Si II (Sembach et al 1995a). This ionization structure is more typical of the high-ionization quasar metal-line absorption systems (see Sargent et al 1979; Steidel 1990) than it is of the quasar mixed-ionization systems, which resemble the absorption characteristics found in the outer Milky Way toward the Magellanic Clouds (Savage & Jeske 1981).

GHRS observations of C IV, N V, and Si IV toward stars in the low halo (Spitzer & Fitzpatrick 1992; Savage & Sembach 1994) and disk (Huang et al 1995) confirm that the high-ionization stages in these regions result primarily from collisional ionization. High-resolution GHRS observations of HD 167756 reveal the presence of C IV and N V at velocities at which no lower ions are detected. This suggests that the C IV and N V absorption occurs in a hot Galactic supershell (Savage et al 1994). Detections of the high ions toward HD 167756 and other stars reveal a second type of highly ionized gas that has lower ionization absorption and that probably traces gas near $T \sim 10^5$ K (see Spitzer 1990 and McKee 1993 for reviews of hot gas in the Galaxy). Rapid progress in theoretical models of conductive interfaces (Borkowski et al 1990) cooling flows (Shapiro & Benjamin 1993), turbulent mixing layers (Slavin et al 1993), and grain destruction in hot regions (Jones et al 1994) eventually may lead to a better understanding of the relationship of ionization and metal abundances in these types of environments.

10. ABUNDANCES IN DIFFUSE CLOUDS

The study of diffuse cloud abundances with the *HST* builds on the pioneering contributions of the *Copernicus* satellite, the use of which demonstrated that many elements in the ISM have lower gas-phase abundances than they do in the Solar System and that the amount of the underabundance (or depletion) depends on sight-line properties (see Jenkins 1987 for a review of the *Copernicus* results). For example, a number of studies (Savage & Bohlin 1979; Murray et al 1984; Harris & Bromage 1984; Harris & Mas Hesse 1986; Jenkins et al 1986; Crinklaw et al 1994) revealed that interstellar depletions correlate much better with average sight-line density $\langle n_{\rm H} \rangle = N({\rm H})/d$ than with total hydrogen column density or total dust extinction. The *Copernicus* observations are not of high enough spectral resolution to help determine gas-phase abundances within individual clouds, but they provide accurate integrated sight-line column densities.

GHRS analyses of correlations with similar quantities that provide indirect information about the presence of dust, such as the molecular fraction of hydrogen $f({\rm H_2}) = 2N({\rm H_2})/[N({\rm H\ I}) + 2N({\rm H_2})]$, confirm that the depletions of some elements are linked to cloud properties. The relationship between dust and $f({\rm H_2})$ is indirect because molecules such as H_2 in interstellar clouds appear to form on grain surfaces (Spitzer 1978), but these molecules are destroyed through processes such as photodissociation without significant dust destruction. In Figure 2 we plot GHRS measurements of O/H, B/H, Zn/H, and Cr/H for sight lines covering a large spread in $f({\rm H_2})$. The dashed line in each panel indicates the solar value of the ratio. The points in the plot sample two regimes: an intercloud or diffuse cloud medium with little molecular material [$f({\rm H_2}) < 0.01$], and a cloudy medium with enough material to shelter molecules from photodissociation by UV starlight [$f({\rm H_2}) > 0.01$]. Although the data points are few, the abundances of O and B are similar over the six-decade range spanned by the measurements, implying that these elements are not readily incorporated into dust in a density-dependent manner. In fact, Meyer et al (1994) postulated that the small deficiency (approximately a factor of two) of interstellar gas-phase O seen toward the four stars shown in Figure 2 could be due to dilution of the ISM by the infall of a metal-poor cloud in the solar neighborhood. This interpretation gains support from the B measurements if the reference abundance is $\log({\rm B/H})_{\rm c} = -9.66$, as found for two F stars (Lemke et al 1993; see also Bosegaard & Heacox 1978). Federman et al (1993) noted that this reference abundance also brings the interstellar B abundance for the ζ Oph sight line into agreement with the abundances of other elements having similar condensation temperatures.

The lack of a trend in the values of O/H and B/H in Figure 2 can be compared with the modest trend (~ 0.5 dex) for Zn/H and the large trend (~ 1.0 dex) for Cr/H between $\log f(H_2) = -6$–0. The more pronounced correlations observed for Zn and Cr are consistent with $f(H_2)$ trends for other elements having modest to large depletions in dense interstellar environments [e.g. Mg (Cardelli 1994) and Fe (Savage & Bohlin 1979)] and with the ensemble of relationships between elemental depletion and sight-line density reviewed by Jenkins (1987). They also provide a basis for linking the observed behavior of gas-dust interactions in the Galaxy with those in quasar absorption-line systems, in which the sight-line density is not easily measured but $f(H_2)$ is known to be low ($\log f(H_2) \lesssim -3$) (Foltz et al 1988; Levshakov et al 1992 and references therein).

The average sight-line density dependence of the elemental depletions in H I regions provided the impetus for a simple explanations for the variations in depletions or gas-phase abundances along different sight lines. Spitzer (1985) proposed that the depletion of an element along a sight line is equal to the average of contributions from three basic types of H I gases: a warm, low-density medium, which predominates at $\langle n_H \rangle \lesssim 0.2$ cm^{-3}; standard diffuse clouds, which contribute most strongly at $\langle n_H \rangle \approx 0.7$ cm^{-3}; and large cold clouds or complexes, the main constituents for sight lines with $\langle n_H \rangle \gtrsim 3$ cm^{-3}. Additional support for this suggestion comes from the work of Joseph (1988), who determined that, for a given level of overall depletion, the sight line-to-sight line variations of the depletions of individual elements are small. If the relative elemental abundances are established early in the lifetime of the grains in the different types of H I regions, then on average this idealized model probably describes well the general character of the neutral ISM.

Although often overused in the ISM literature as a typical interstellar sight line, the ζ Oph line of sight ($l = 6.3^\circ$, $b = +23.4^\circ$, $d = 140$ pc) presents an excellent example of the dependence of elemental depletions on cloud types. In Figure 3 we show high-resolution (FWHM = 3.5 km s^{-1}) GHRS spectra of various interstellar lines in the ζ Oph spectrum. The two main clouds (or groups of clouds) along the sight line at $v_{helio} = -27$ and -15 km s^{-1}, respectively, are easily separated in this echelle data and clearly have different ion-to-ion absorption strengths owing to differences in their physical conditions (n_H, T, etc). The cloud at -27 km s^{-1} is warm and has properties consistent with those of the warm neutral medium. The cloud(s) at -15 km s^{-1} contain(s) molecules and resembles a blend of cool diffuse clouds and a large cold cloud.

The left panel of Figure 3 contains a series of interstellar lines for elements that range from lightly depleted (N I, O I) to moderately depleted (Mg II, Mn II) to highly depleted (Fe II, Ni II, Cr II). In this progression, the warm cloud absorption strength increases relative to the cool cloud absorption strength

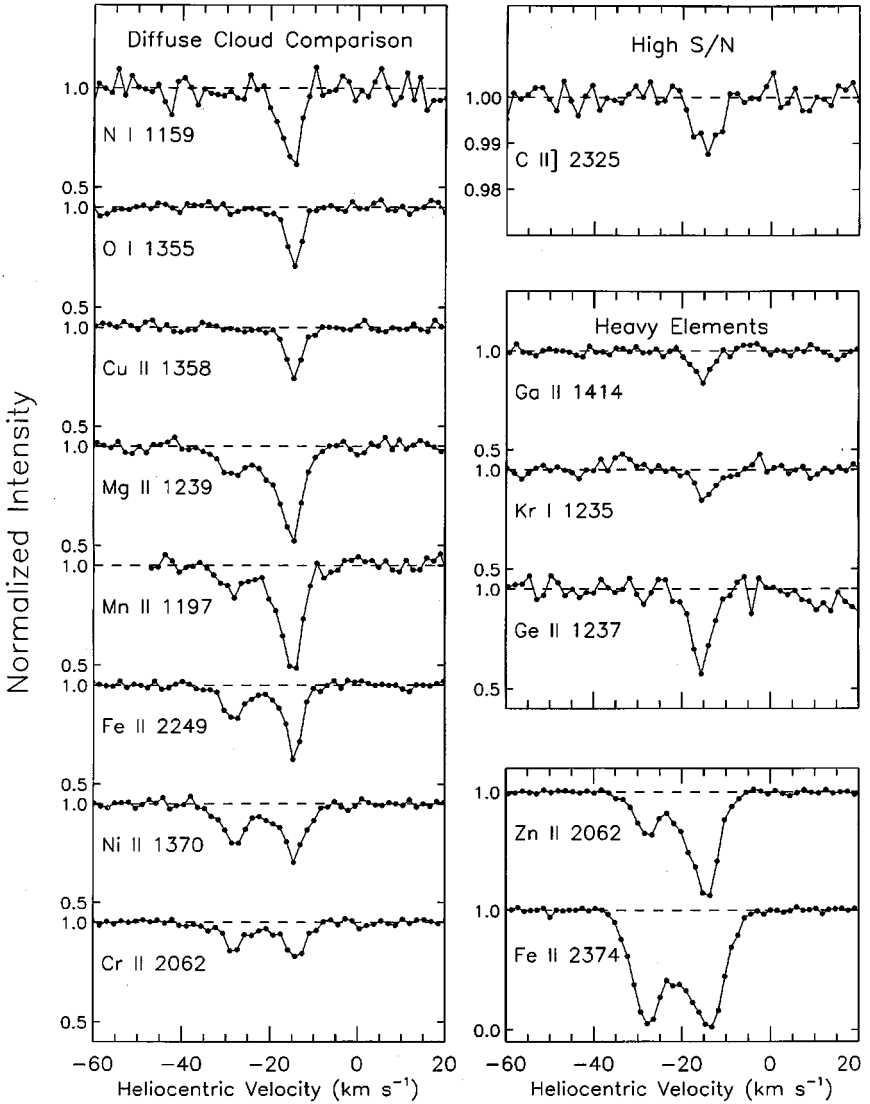

Figure 3 Continuum normalized profiles for selected interstellar lines in the direction of ζ Oph. The left panel shows a series of weak lines of elements that are lightly depleted (N I, O I, Cu II), moderately depleted (Mg II, Mn II), and highly depleted (Fe II, Ni II, Cr II). The bottom right panel shows stronger lines for a weakly depleted (Zn II) and a highly depleted (Fe II) element. The absorption near -27 km s^{-1} is tracing gas in a warm neutral cloud with $\log N(\mathrm{H}) = 19.74$ while the absorption near -15 km s^{-1} is tracing a cool diffuse cloud with $\log N(\mathrm{H}) = 21.12$ (see Table 5). The upper right panel shows a high S/N observation of the C II] line at 2325 Å. This weak line is valuable in determining reliable column densities of C in the ISM (see Cardelli et al 1993c). The middle right panel shows several examples of weak-line detections of heavy ($Z > 30$) elements toward ζ Oph. Note that the vertical scales in all panels are not identical.

Table 5 Gas-phase abundances in the diffuse clouds toward ξ Persei and ζ Ophiuchi[a,b,c]

			[X/H] = log(X/H) − log(X/H)$_\odot$ $(+1\sigma, -1\sigma)$				
			ξ Persei	ζ Ophiuchi			
	log(X/H)$_\odot$[d]	T_c[e]	Cool	Cool	Warm	Ref.[f]	Note[g]
Li	-8.69	1225	...	-1.58 (0.05,0.05)	...	1	1
B	-9.12	650	...	-0.93 (0.07,0.09)	...	9	2
C	-3.45	75	-0.16 (0.11,0.14)	-0.41 (0.08,0.13)	...	7	3
N	-4.03	120	...	-0.07 (0.05,0.06)	...	5	
O	-3.13	180	-0.39 (0.05,0.06)	-0.39 (0.04,0.06)	0.00 (0.18,0.31)	5,7	
Na	-5.69	970	...	-0.95 (0.10,0.10)	...	1	1
Mg	-4.42	1340	-1.24 (0.04,0.04)	-1.55 (0.02,0.03)	-0.89 (0.05,0.05)	3,4,5	4
Si	-4.45	1311	> -1.26	-1.31 (0.03,0.03)	-0.53 (0.01,0.01)	4,5,10,13	5,6
P	-6.43	1151	-0.61 (0.02,0.03)	-0.50 (0.16,0.24)	-0.23 (0.02,0.02)	3,4,12	10
S	-4.73	648	> -1.05	+0.18 (0.17,0.30)	...	4,9	6,7
Cl	-6.73	863	...	0.00 (0.20,0.20)	...	1	
Ar	-5.44	25	...	-0.48 (0.16,0.16)	...	1	
K	-6.87	1000	...	-1.09 (0.24,0.25)	...	1	1
Ca	-5.66	1518	...	-3.73 (0.04,0.06)	...	1	1
Ti	-7.07	1549	-2.59 (0.05,0.05)	-3.02 (0.03,0.04)	-1.31 (0.06,0.08)	2,5	8
V	-7.98	1450	...	< -1.96	...	12	9
Cr	-6.32	1277	-2.08 (0.01,0.02)	-2.28 (0.03,0.03)	-1.07 (0.04,0.04)	3,4,5	
Mn	-6.47	1190	-1.32 (0.02,0.03)	-1.45 (0.03,0.03)	-0.90 (0.05,0.05)	3,4,5	
Fe	-4.49	1336	-2.09 (0.03,0.03)	-2.27 (0.02,0.03)	-1.25 (0.03,0.04)	3,4,5	
Co	-7.09	1351	...	-2.76 (0.10,0.12)	-1.54 (0.13,0.19)	9	
Ni	-5.75	1354	-2.46 (0.04,0.05)	-2.74 (0.02,0.02)	-1.51 (0.03,0.03)	3,4,5	
Cu	-7.73	1037	-1.53 (0.06,0.07)	-1.35 (0.03,0.02)	-0.82 (0.13,0.17)	3,4,5	
Zn	-7.35	660	-0.64 (0.02,0.02)	-0.67 (0.11,0.11)	-0.03 (0.02,0.01)	3,4,12	11
Ga	-8.87	918	...	-1.14 (0.06,0.06)	...	5	
Ge	-8.37	825	-0.67 (0.08,0.11)	-0.62 (0.04,0.04)	...	5,8	
As	-9.63	1157	...	-0.21 (0.09,0.09)	...	6	
Se	-8.65	684	...	+0.10 (0.23,0.23)	...	6	
Kr	-8.77	25	...	-0.26 (0.06,0.07)	...	5	
Sn	-9.86	720	...	+0.02 (0.09,0.09)	...	6	
Te	-9.76	680	...	< +0.77	...	6	
Tl	-11.18	450	...	+0.45 (0.12,0.12)	...	11	
Pb	-9.95	520	...	-0.71 (0.15,0.15)	...	11	

[a] Values of [X/H] = log(X/H) − log(X/H)$_\odot$ for elements in italics are from *Copernicus* or ground-based measurements. All others are from GHRS measurements.

[b] Log N(H) = 21.30 ± 0.17 for the cool diffuse clouds towards ξ Per. Log N(H) = 21.12 ± 0.10 for the cool diffuse clouds toward ζ Oph. Log N(H) = 19.74 for the warm diffuse cloud(s) toward ζ Oph. This value is derived by holding the O and Zn abundances in the cloud to within ≈10% of solar abundances (see Savage et al 1992) and is consistent with 21-cm measures of the sight line (Cappa de Nicolau & Poppel 1986). The uncertainty in N(H) for the component is probably ≈ 0.2–0.3 dex.

[c] All values of [X/H] have been converted into the system of atomic constants and reference abundances used throughout this paper. Errors ($\pm 1\sigma$) are based on measurement errors N(X) only and do not include uncertainties in N(H), solar reference abundances, or atomic constants. Limits are 2σ estimates.

[d] Reference solar abundances, derived from meteoritic data, except for C, N, and O, which are derived from solar photosphere data (Grevesse & Noels 1993). The typical error (1σ) in these values is ≈ 0.04 dex (see Table 1).

[e] Condensation temperatures appropriate for the solar nebula with an initial gas pressure of 10^{-4} atm. The condensation temperature is the temperature at which 50% of the element has been removed from the gas phase. All values are from Wasson (1985 and references therein), except those for Pb and Tl (Grossman & Larimer 1974); C, N, O, Ar (Field 1974); and Kr (which we assume to be equal to the value for Ar). The noble gases Ar and Kr may be removed from the gas phase at temperatures between 450 and 700 K through solubility in magnetite (Lancet & Anders 1973; Grossman & Larimer 1974), which may help explain their modest subsolar abundances.

[f] ξ Per and ζ Oph abundance references: (1) Morton 1975 and references therein; (2) Stokes 1978; (3) Cardelli et al 1991b; (4) Savage et al 1991; (5) Savage et al 1992; (6) Cardelli et al 1993b; (7) Cardelli et al 1993c; (8) Cardelli et al 1991a; (9) Federman et al 1993; (10) Cardelli et al 1994; (11) Cardelli 1994; (12) New result derived for this article; (13) Sofia et al (1994).

because of the dependence of the elemental depletions on cloud conditions. For example, the O I absorption is hardly detected in the warm cloud compared to the cool cloud which is consistent with the H I column density being approximately ten times smaller in the warm cloud than in the cool cloud. In contrast, the Cr II absorption at the bottom of the panel has comparable strength in the two clouds. Cr II is lightly depleted in the warm cloud and heavily depleted in the cool cloud. A similar example between the strong lines of a lightly depleted element (Zn II) and a highly depleted element (Fe II) is shown in the lower right panel of Figure 3. Savage et al (1992) interpreted the depletion behavior and physical condition differences within the two clouds as direct evidence for Spitzer's (1985) model explaining the mean density dependence of interstellar depletions.

In Table 5 we list values of $[\mathrm{X/H}] = \log(\mathrm{X/H}) - \log(\mathrm{X/H})_\odot$ observed in the cool and warm diffuse clouds toward ζ Oph by the GHRS together with values observed in the cool diffuse clouds toward another well-studied object, ξ Per ($l = 160.4^\circ, b = -13.1^\circ, d = 540$ pc). We converted all gas-phase abundances into our preferred system of atomic constants (see Section 5) using the solar reference abundances listed in the second column of the table. The errors on [X/H] reflect measurement errors in $N(\mathrm{X})$ only and do not account for uncertainties in oscillator strengths or reference abundances. Changes in [X/H] due to errors in $N(\mathrm{H})$ are systematic across all elements. Errors for $N(\mathrm{H})$ are given in footnote b of Table 5; the value of $N(\mathrm{H})$ for the warm cloud toward ζ Oph is particularly uncertain. The condensation temperature listed in the third column of Table 5 is the temperature at which half of the initial amount of an element is removed from a gas of solar composition owing to the formation of solid matter under conditions close to thermal and chemical equilibrium. The values of T_c are appropriate for a solar nebula with an initial pressure of 10^{-4} atmospheres (Wasson 1985). For lower initial pressures, the values of T_c are larger but are generally within a few tens of degrees of the listed values. For some refractory elements, such as Fe, the differences may be as large as 150° if the initial pressures are as low as 10^{-6} atm (see Wai & Wasson 1977).

[g]Notes: (1) Abundance for ζ Oph cool cloud derived from trace ionization stage and ionization equilibrium considerations, with $n_e = 0.7$ cm^{-3} and $T = 56$ K; (2) Federman et al (1993) prefer $\log(\mathrm{B/H})_\odot = -9.66$ based on the work of Lemke et al (1993); (3) [C/H] determined from weak C II λ2325 intersystem line; (4) The f-values of the Mg II $\lambda\lambda$1239.9, 1240.4 lines still may contain substantial uncertainties; (5) [Si/H] for the ζ Oph cool cloud agrees with the value obtained from the weak Si II] λ2335 intersystem line; (6) Lower limit for ξ Per derived from profile integration of moderately saturated line; (7) ζ Oph result based on observations of SI and ionization balance considerations; (8) Result based on the optical line at 3384 Å (Stokes 1978); (9) Derived from a measured upper limit of 1.0 mÅ for the V II line at 2683.887 Å using an f-value of 0.1026; (10) The ζ Oph cool cloud P II value is derived from component fitting to the line at 1152.818 Å. Measurements of the weaker line at 1532.533 Å would enable stronger constraints to be placed on the P II abundance in the cloud; (11) The ζ Oph cool cloud Zn II value is derived from component fitting to the lines at 2036.136 and 2062.664 Å. This result improves on the previously published estimate of [Zn/H].

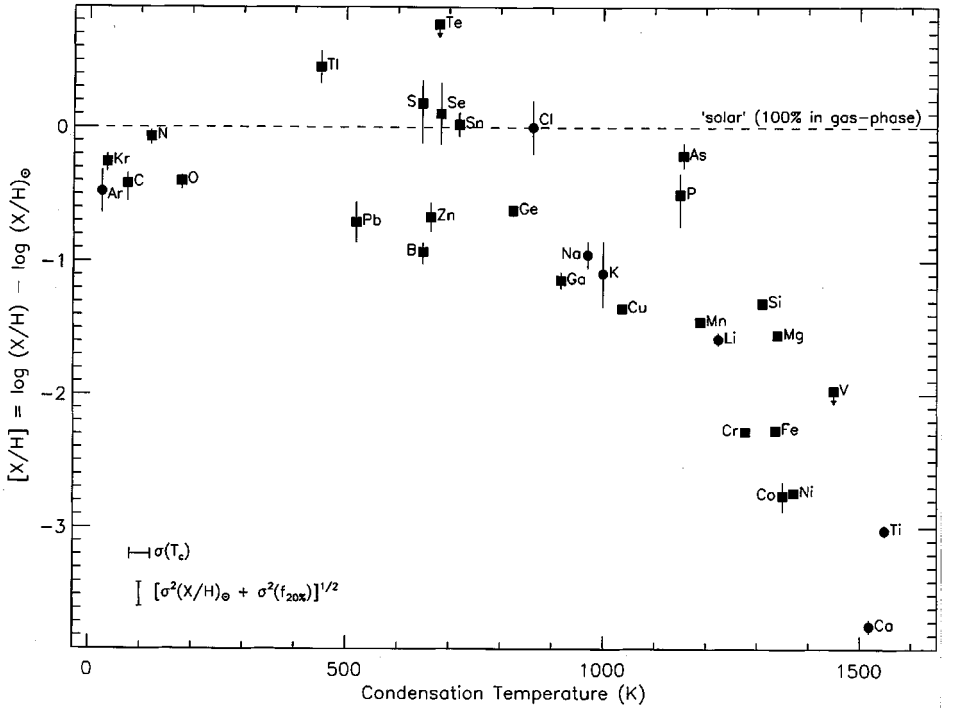

Figure 4 Gas-phase abundance, $[X/H] = \log(X/H) - \log(X/H)_\odot$, vs condensation temperature for the cool diffuse interstellar cloud toward ζ Oph. The data used to construct this plot are listed in Table 5. The condensation temperature is the temperature at which 50% of an element has been removed from the gas phase. GHRS data points referenced to solar abundances are shown as filled squares. *Copernicus* satellite and optical data points are indicated by filled circles. The error bars on all points represent measurement errors only. The data points for Kr and Ni have been shifted slightly in the horizontal direction for clarity. The 1σ errors in condensation temperature (± 20 K) and solar reference abundances combined with f-value uncertainties (± 0.04 dex) are shown in the lower left corner of the plot.

In Figure 4 we present the cool diffuse cloud abundance results for ζ Oph plotted in the familiar form of gas-phase abundance vs condensation temperature. The GHRS data (*filled squares*) are supplemented by *Copernicus* and ground-based observations (*filled circles*) for a few elements. In the cool cloud, C, N, O, S, Ar, Kr, and some heavy elements have depletion factors of less than three. P, Zn, and Ge have slightly larger depletion factors. Ca, Ti, V, Cr, Fe, Co, and Ni have depletion factors in excess of 100. This is the most complete set of elemental abundances available for any interstellar cloud. The depletion pattern exhibited by this cloud, in which elements with larger condensation

temperatures generally have greater depletion factors as well, was first studied by Field (1974), who noted that the abundance deficiencies generally correlate with the temperatures derived for particles condensing out of the gas phase in cool stellar atmospheres. Since then it has become increasingly clear that the correlation of depletion with T_c also may depend on (or be lessened by) the growth of grains in molecular clouds and their subsequent stripping and destruction by shocks in the warm ISM. Time-scale considerations (Draine 1990) show that most grains experience at least one period of regrowth in the ISM during their lifetime and that the extreme depletion of various elements created in supernova explosions (such as Ca, Ti, Fe) can be explained only by elemental condensation within molecular clouds unless $>$ 99.9% of the interstellar gas is cycled through a cool star atmosphere or through a surrounding nebula (Jenkins 1987). This realization is reinforced by the different depletions and properties of the two ζ Oph clouds. A more complete discussion of the origin and evolution of interstellar grains can be found in the monograph by Whittet (1992).

Figure 5 is a graphical comparison of the abundance results for the two ζ Oph diffuse clouds for those elements measured in both. For clarity of presentation, the ordering of the figure is one of decreasing abundance or increasing depletion factor. The differences in the gas-phase abundances within the two clouds are small (< 0.5 dex) for lightly depleted elements such as O and large (> 1 dex) for heavily depleted refractory elements such as Fe and Cr. The lower dashed line in the figure indicates the neutral hydrogen column density–weighted averages of the abundances within the ζ Oph clouds, which are dominated by the cool cloud values. The cool cloud values listed in Table 5 for the ξ Per sight line are close to the ζ Oph average values for many elements, indicating that the integrated sight-line values for the diffuse clouds along these two directions are likely similar as well. The cool clouds toward ξ Per show a velocity-dependent depletion effect that may result from the mixing of different interstellar gases. For example, between $v_{\rm helio} = +5$ and $+20$ km s^{-1}, the Cr and Fe abundances relative to Zn and O increase by a factor of two (Cardelli et al 1991b; Savage et al 1991), suggesting that this absorption traces a mixture of cloud types.

In addition to providing the velocity resolution necessary to distinguish the absorptions in different interstellar clouds, the GHRS, through its ability to obtain high S/N data, can detect weak lines of cosmically abundant elements (in some cases even those with large depletion factors) or large f-value lines of elements with low cosmic abundances. Such studies have extended the basic interstellar detection list established by *Copernicus* to include elements as heavy as Pb ($Z = 82$; see Table 1). An example of the high S/N spectrum for the C II] λ2325 line toward ζ Oph from Cardelli et al (1993c) is shown in the top right

panel of Figure 3. This weak line, which provides an example of the type of data necessary to detect weak intersystem lines of abundant elements (see also Meyer et al 1994), is particularly useful for establishing the C abundance in the interstellar medium because the resonance line of C II near 1334 Å is very strong and is almost always too saturated to yield a reliable carbon abundance. The absorption lines of rare elements also often have equivalent widths of less than 1 mÅ and must have high S/N ratios in order to be detected. Examples of weak-line detections for several heavy elements (Ga II, Ge II, Kr I) for the ζ Oph sight line are shown in the middle right panel of Figure 3. Heavy elements such as these (and others such as As, Sn, Te, Tl, and Pb) extend the study of interstellar chemical behavior into the fifth and sixth rows of the periodic table and provide information

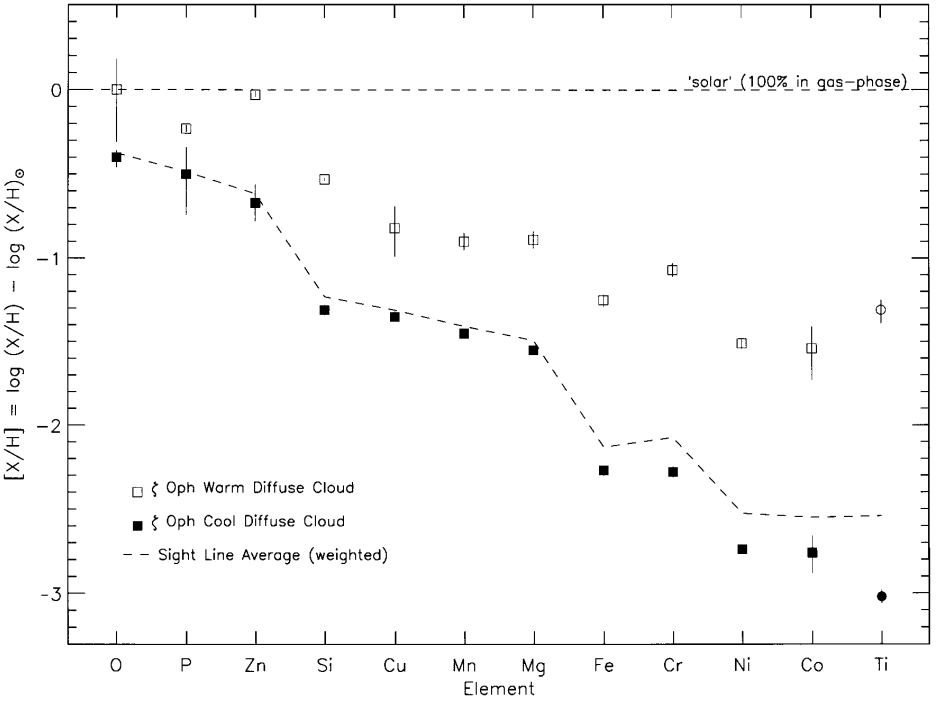

Figure 5 A comparison of the gas-phase abundances, [X/H] = log(X/H) − log(X/H)$_\odot$, in the cool and warm diffuse clouds toward ζ Oph at heliocentric velocities of -15 km s^{-1} and -27 km s^{-1}, respectively. The elements are arranged in order of decreasing gas-phase abundance (which is approximately one of increasing condensation temperature). The dashed line indicates the column density-weighted sight-line average abundances. There is a general progression in abundance differences as a function of elemental depletion (see text). The data used to construct this plot are listed in Table 5.

Table 6 Summary of diffuse cloud gas-phase abundances for cosmically abundant elements[a]

	[X/H] = log(X/H) − log(X/H)$_\odot$						
Cloud type[b]	Mg	Si	S	Mn	Cr	Fe	Ni
Halo	(<-0.28,-0.56)	(-0.09,-0.47)	(-0.23,+0.16)	(-0.47,-0.72)	(-0.38,-0.63)	(-0.58,-0.69)	(-0.77,-0.91)
Disk+ Halo	(-0.59,-0.62)	(-0.23,-0.28)	(+0.03)	(-0.66)	(-0.72,-0.88)	(-0.80,-1.04)	(-1.15)
Warm Disk	(-0.73,-0.90)	(-0.35,-0.51)	(-0.03,+0.14)	(-0.85,-0.99)	(-1.04,-1.15)	(-1.19,-1.24)	(-1.44,-1.48)
Cool Disk	(-1.24,-1.56)	(-1.31)	(~ 0.00)	(-1.32,-1.45)	(-2.08,-2.28)	(-2.09,-2.27)	(-2.46,-2.74)

[a]The values listed for each element represent the range of [X/H]= log(X/H) − log(X/H)$_\odot$ found by Sembach & Savage (1996) for each type of cloud. For some sight lines in the halo, disk + halo, and warm disk categories we assumed [X/H] ≈ [X/Zn] ≈ [X/S] since no H I or H_2 estimates were available for the individual clouds studied. Zn and S are nearly undepleted in such environments. When only one value is listed, the element was measured for only one sight line.

[b]Halo cloud sight lines: HD 38666 ($v_{\rm helio} = 41$); HD 93521 ($v_{\rm helio} < -22$); HD 116852 ($v_{\rm helio} = -29$ to -64 and -4 to -29); HD 149881, 3C 273. Disk + halo cloud sight lines: HD 18100, HD 167756. Warm disk cloud sight lines: HD 38666 ($v_{\rm helio} = 23$), HD 93521 ($v_{\rm helio} > -22$), HD 149757 ($v_{\rm helio} = -27$). Cool disk cloud sight lines: HD 24912 ($5 < v_{\rm helio} < 20$), HD 149757 ($v_{\rm helio} = -15$).

about r- and s-process nucleosynthesis enrichment of the ISM or about rare elements not previously detected in interstellar clouds (Cardelli et al 1991a; Hobbs et al 1993; Cardelli 1994; Wallerstein et al 1995b; Welty et al 1995).

The GHRS has been used to study individual diffuse clouds along many different lines of sight through the Milky Way disk and halo. These sight lines exhibit various elemental mixes and different types of diffuse clouds. For example, the 1.7-kpc sight line to the low halo star HD 93521 intersects nine distinct warm interstellar clouds ($T \sim 6000$ K) and one cool interstellar cloud ($T \sim 500$ K) (Spitzer & Fitzpatrick 1993). Spectra for several interstellar lines in this direction are shown in Figure 1. The abundances within the warm diffuse clouds toward HD 93521 depend in part on the velocities of the clouds. The warm slow clouds, which have $|v_{\rm helio}| \lesssim 10$ km s^{-1} and are located in the Galactic disk, have depletions very similar to those of the warm diffuse cloud toward ζ Oph (see Figure 5). The faster-moving warm clouds with $|v_{\rm helio}| \gtrsim 35$ km s^{-1} are located in the low halo and have abundances closer to solar abundances and to those of other halo clouds than do the slow clouds. The velocity dependence of the depletions along the HD 93521 sight line is probably due to acceleration of the higher-velocity clouds by shocks that destroy a portion of the dust within the clouds (see Section 14 and Spitzer & Fitzpatrick 1993).

To provide a summary of the diffuse cloud depletions in different environments, we assembled the available GHRS data for nine sight lines in Table 6, where we list [X/H] for several abundant elements (e.g. Mg, Si, S, Mn, Cr, Fe, and Ni). Information for C, N, and O is provided in Section 12 for selected sight lines. The sight lines fall into four general classes divided into disk and halo regions. The two numbers for each element represent the observed range in values of [X/H]. For some of the warm clouds, we use values of [X/Zn] or

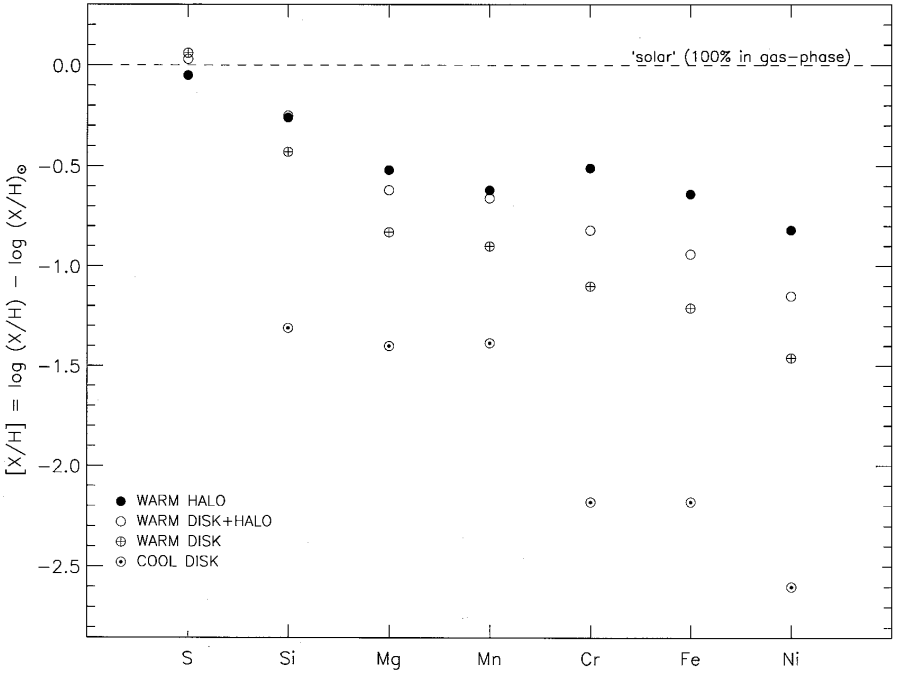

Figure 6 Gas-phase abundances, [X/H] = log(X/H) − log(X/H)$_\odot$, of 7 abundant elements for diffuse cloud sight lines in the Galactic disk and halo. The values of [X/H] for halo clouds have been derived from measures of [X/Zn] and the assumption that [X/Zn] ∼ [X/H]. The data used to construct this figure are in Table 6. The cool disk data points are averages for the cool diffuse clouds toward ξ Per and ζ Oph (Table 5). Note the clear differences in the abundance patterns of the disk and halo gases. The upper envelope of abundances established by the halo cloud values indicates that the halo clouds contain a substantial amount of dust with core material that is difficult to destroy through the processes that inject gas and dust into the halo.

[X/S] from Sembach & Savage (1996) as measures of [X/H] since Zn and S have nearly solar abundances relative to H for these types of clouds (Harris & Mas Hesse 1986; Spitzer & Fitzpatrick 1992, 1995; Sembach et al 1995b; Roth & Blades 1995) and since accurate H I information was unavailable for most individual clouds studied. The elemental abundances of diffuse clouds in these regions exhibit systematic differences. Figure 6 shows the average gas-phase abundances for the halo and disk cloud sight lines listed in Table 6. Systematic differences of this type provide new insight into the physical processes that process dust and transport gas within the Galaxy. For the first time in interstellar studies, halo cloud abundances can be studied in as great detail as nearby disk clouds. We discuss Figure 6 and its implications further in Section 13.

11. ISOTOPIC AND MOLECULAR ABUNDANCES

11.1 *The Abundance of Deuterium*

Deuterium in interstellar gas can be atomic or chemically combined in molecules such as HD. Because fractionation affects the molecular abundance of D, the best way to obtain the interstellar ratio of D to H is through direct measures of atomic D I and H I. The larger mass of D compared with H shifts the UV Lyman series absorption of D I by -81.55 km s^{-1} from the Lyman series of H I. The *Copernicus* satellite provided the first reliable measures of the D-to-H ratio in the ISM and produced a large data base of D I and H I Lyman series observations (Rogerson & York 1973; York & Rogerson 1976). In a reanalysis of the *Copernicus* data and of measurements from the *IUE* satellite, McCullough (1992) estimated the mean value of the D-to-H ratio in the local interstellar medium to be $(D/H)_{LISM} = (1.5 \pm 0.2) \times 10^{-5}$ and found no evidence of changes in the ratio from cloud to cloud. However, this result is not universally accepted (Laurent et al 1979; Bruston et al 1981), and higher-precision abundance measurements are required in order to reduce the errors.

Linsky et al (1993, 1995) used the GHRS to obtain an accurate measure of the D-to-H ratio toward Capella, a binary star system at a distance of 12.5 pc. They obtained high S/N observations of the Lyα lines of D I and H I at near opposite orbital quadratures, thus enabling accurate derivations of both the stellar Lyα line profiles and the interstellar H I and D I absorption lines. The full-profile analysis for the direction to Capella yields $(D/H)_{LISM} = 1.60 \times 10^{-5}$, with 1σ random errors of $\pm 0.09 \times 10^{-5}$ and systematic errors of $(+0.05, -0.10) \times 10^{-5}$ (Linsky et al 1995). GHRS observations obtained for the sight line to Procyon ($d = 3.5$ pc) by the same investigators are consistent with the Capella result, but the shape of the intrinsic stellar Lyα profile prevents them from setting stronger constraints on the constancy of the D-to-H ratio in the LISM.

Because Galactic chemical evolution destroys D, the Capella sight-line result $(D/H)_{LISM} \geq 1.41 \times 10^{-5}$ sets a strong lower limit on the primordial D abundance. This limit, together with standard Big Bang nucleosynthesis calculations that assume a cosmological constant of zero (Walker et al 1991; Dar 1995), places a strong upper limit on the local baryon density of $\Omega_B h_{50}^2 \lesssim 0.125$, where Ω_B is the ratio of the local baryon density to the critical density and h_{50} is the Hubble constant in units of 50 km s^{-1} Mpc^{-1}. A smaller upper limit of $\Omega_B h_{50}^2$ is implied by the value of D/H $\approx (1.9$–$2.5) \times 10^{-4}$ reported by Songaila et al (1994), which is based on the analysis of a Keck Observatory spectrum of a QSO absorption line system at $z = 3.32015$ toward Q0014 + 813. The D-to-H ratio must be observed in a number of astrophysical sites with a range

of metallicities in order to determine its primordial value and to rule out the possibility that particular candidate D I lines are H I Lyα forest lines.

11.2 *The Molecular Fractionation of the Isotopes of C and O*

UV absorption-line studies of CO provide an opportunity to examine the isotopic fractionation of C and O associated with various molecule formation and destruction processes in diffuse interstellar clouds. For example, the fractionation of CO is quite severe in the diffuse cloud toward ζ Oph – $^{12}CO/^{13}CO \approx 167$, $C^{16}O/C^{18}O \approx 1550$, and $C^{16}O/C^{17}O > 5900$ (Lambert et al 1994). These molecular ratios are larger than atomic isotopic ratios of O for the Sun ($^{16}O/^{18}O \approx 500$ and $^{16}O/^{17}O \approx 2600$; Anders & Grevesse 1989) or of C for the ζ Oph sight line ($^{12}C/^{13}C \approx 66$). The $^{12}C/^{13}C$ ratio for ζ Oph is derived from optical measures of $^{12}CH^+/^{13}CH^+ \approx 66$ and from the assumption that isotopic fractionation does not affect CH^+ since the molecule is produced in warm gas and photodissociation of the two species is nonselective (Crane et al 1991; Hawkins et al 1993).

Two basic processes affect isotopic fractionation in the CO molecule: ion-molecule charge-exchange reactions and selective photodissociation. The ion-molecule charge-exchange reaction

$$^{13}C^+ + {}^{12}CO \leftrightarrow {}^{13}CO + {}^{12}C^+ + \Delta E \tag{8}$$

is exothermic and favors the production of ^{13}CO relative to ^{12}CO. However, photodissociation of ^{12}CO and ^{13}CO favors the selective destruction of ^{13}CO since self-shielding is more effective for the more abundant ^{12}CO molecule. The observed ratio $^{12}CO/^{13}CO \approx 167$ therefore provides information about the effectiveness of the two competing processes. Selective photodissociation appears to dominate the equilibrium ratio of the two species, which means that the standard models for the conditions in the well-studied diffuse cloud in front of ζ Oph must be revised (Lambert et al 1994). Ion-molecule charge-exchange reactions do not influence the equilibrium balance involving the different isotopes of O in the CO molecule since the dominant form of O in diffuse clouds is neutral. However, selective photodissociation leads to molecular fractionation, as is observed.

11.3 *Molecular Abundances*

Wavelength identifications and f-values for many molecules with electronic transitions in the GHRS spectral range can be found in Jenkins et al (1973) and van Dishoeck & Black (1986). Apart from the isotopically substituted molecules discussed above, to date the only new discoveries of molecular interstellar species with the GHRS are tentative detections of HCl and vibrationally excited H_2.

Federman et al (1995) reported a tentative 2.5σ detection of the HCl C-X (0-0) R(0) 1290.257 Å line toward ζ Oph. Column density estimates for Cl, Cl^+, H_2, and HCl provide a meaningful check on diffuse cloud chemical models describing the formation of HCl through reactions involving Cl^+ and H_2. The Federman et al model for the conditions in the neutral, diffuse cloud toward ζ Oph, which is based on a previous model by van Dishoeck & Black (1986), adequately predicts the observed column densities for Cl, H_2, and HCl. The inability of the model to predict the Cl^+ column density to within a factor of approximately three has led the investigators to suggest that the observed value of $N(Cl^+)$ for the cloud might be contaminated by Cl^+ absorption from the H II region surrounding the star.

The *Copernicus* satellite revealed that H_2 is the most abundant molecule in interstellar space with typical fractional abundances $f(H_2) = 2N(H_2)/[N(H\ I) + 2N(H_2)]$ of ≈ 0.2 toward stars with B-V color excesses of approximately 0.3 magnitudes (Savage et al 1977). Spitzer et al (1974) studied in detail the rotational excitation of H_2 up to $J = 6$, but the search for vibrationally excited H_2 with *Copernicus* was unsuccessful (Frisch & Jura 1980). Detections of vibrationally excited H_2 created by fluorescent pumping by UV radiation would yield information about the rate of pumping and the mean intensity of UV radiation in diffuse clouds. Federman et al (1995) reported tentative 2σ detections of the H_2 B-X(0-3) R(0) and R(1) lines at 1274.537 and 1274.922 Å in the diffuse clouds toward ζ Oph. Confirmation of these detections would imply $H_2(v = 3)$ column densities a factor of two to three times smaller than the detailed model predictions of van Dishoeck & Black (1986) and a less intense radiation field than is usually assumed. Such detailed checks on the gas and radiation conditions in the ζ Oph clouds are important since this well-studied interstellar sight line provides many critical tests of theories of interstellar atomic and molecular processes.

12. IMPLICATIONS FOR THE COMPOSITION OF INTERSTELLAR DUST

Measures of the gas-phase abundances (g) of the elements in interstellar clouds provide indirect information about the composition of the interstellar dust (d), provided the total (gas + dust) or cosmic abundance (c) is known. The assumption

$$(X/H)_d = (X/H)_c - (X/H)_g \tag{9}$$

allows the absolute and relative numbers of atoms incorporated into grains found in various types of interstellar clouds to be determined. Studies of the

most abundant elements (such as C, N, O, Si, S, Mg, and Fe) yield information about the primary grain constituents, whereas knowledge of the rarer elements provides insight into the processes by which different types of atoms are incorporated into and removed from interstellar grains. As discussed in Section 8, we adopt $(X/H)_c = (X/H)_\odot$, but we also study the implications of using cosmic reference abundances appropriate for the elements found in young main-sequence B stars by assuming $\log(X/H)_{B\ star} = \log(X/H)_\odot - 0.20$.

By measuring the gas-phase abundances in individual interstellar clouds with the GHRS, we can determine dust-phase abundances in clouds of different types and study the composition of dust with different histories of formation and destruction. In our discussions of dust composition, we assume that dust grains found in cool diffuse clouds consist of resilient grain cores covered with mantles. This assumption is consistent with many of the current theoretical ideas about dust formation, growth and destruction (Barlow & Silk 1977; Barlow 1978a,b; Joseph 1988; Mathis 1990) and is supported by the new GHRS observations (see Section 10 and below).

12.1 *Composition of Grain Cores and Mantles*

Dust-phase abundances measured for individual interstellar clouds yield information about the overall composition of dust (core + mantle) in the cloud. We summarize the dust-phase abundances of important elements in several types of interstellar clouds in Table 7, in which we list values of $10^6(X/H)_d$, the dust-phase atomic abundances. This quantity refers to the number of atoms of X in the dust compared to H in the gas. For example, $10^6(O/H)_d = 450$, implies a dust phase O abundance of 450 atoms compared to 10^6 H atoms in the gas.

The left half of the table lists dust composition values derived using solar abundances from Table 1 as the reference cosmic abundance, and the right half of the table lists dust composition values derived using B-star abundances as the cosmic reference standard. The dust-phase abundances given for the cool diffuse clouds toward ζ Oph and ξ Per provide information about the composition of grain cores and mantles, whereas the average results for the warm halo clouds likely represent measures of dust-phase abundances in resilient dust grain cores stripped of their mantles (see Figure 6). In this section we concentrate on results for the combined effects of mantles and cores and examine results for the cool clouds toward ζ Oph and ξ Per.

OXYGEN GHRS determinations of the abundance of oxygen improve on the earlier *Copernicus* survey results based on the weak O I] λ1355 line, which showed that O has a subsolar abundance in the ISM (York et al 1983). Sofia et al (1994) found that the weak O I] λ1355 and damped O I λ1302 lines yield similar column densities, indicating that the unexpectedly low interstellar gas-phase O

abundances measured by *Copernicus* and the GHRS cannot be attributed to problems with the oscillator strength of the weak line. If the solar O abundance is used as the reference abundance, then ~ 450 O atoms per 10^6 H atoms must reside in the dust. The only other atoms with cosmic abundances adequate to combine chemically with this much O are H and possibly C. However, the interstellar H_2O ice feature at 3.1 μm is not seen in absorption along paths through diffuse interstellar clouds. For example, toward VI Cyg No. 12, the absence of the ice band (Sandford et al 1991) implies that less than 0.02% of O is in the form of ice. This problem of the "missing" O can be eased substantially, but not completely eliminated, if a B-star reference abundance of 0.20 dex less than the solar abundance is adopted. In this case, ~ 170 O atoms per 10^6 H atoms could be chemically incorporated into silicates and various oxides of Mg and Fe in the grains. If we adopt the full 0.25-dex difference between the B-star and solar O abundances given in Table 4, the problem of the missing O is resolved. The values of O/Si in the grains toward ζ Oph are 13 and 8 for solar and B-star reference abundances, respectively. If the grains were pure silicates, the expected value would be between three and four. Some of the O is evidently in the form of oxides (see Section 12.2). In the C1 carbonaceous chondrites, the value of O/Si is eight (Whittet 1984; Wasson & Kallemeyn 1988). Correcting for the O combined with H in the meteoric material, which presumably is in

Table 7 Dust-phase abundances[a]

	10^6(X/H)	10^6(X/H)$_d$				10^6(X/H)	10^6(X/H)$_d$			
X	Sun	ζ Oph (core + mantle)[b]	ξ Per (core + mantle)[b]	Halo (core)[c]	(mantle)[d]	B-Star	ζ Oph (core + mantle)[b]	ξ Per (core + mantle)[b]	Halo (core)[c]	(mantle)[d]
O	740	450	440	…	…	470	170	170	…	…
C	360	220	110	…	…	220	89	0.0	…	…
N	93	14	…	…	…	59	0.0	…	…	…
Mg	38	37	36	27	10	24	23	22	12	10
Si	36	34	<34	16	18	23	21	<20	2.9	18
Fe	32	32	32	25	7.0	20	20	20	13	7.0
S	19	0.0	<17	2.0	0.0	12	0.0	<10	0.0	0.0
Ni	1.8	1.8	1.8	1.5	0.3	1.1	1.1	1.1	0.87	0.23
Cr	0.48	0.48	0.48	0.33	0.15	0.30	0.30	0.30	0.15	0.15
Mn	0.34	0.33	0.32	0.26	0.07	0.21	0.20	0.20	0.13	0.07

[a]Dust-phase element abundances are listed in the units 10^6 (X/H)$_d$ for solar reference abundances (left side of table; see Table 1) and B-star reference abundances (right side of table; see Section 8). The reference is to the amount of H in the gas. Therefore, the value 10^6 (X/H)$_d$ = 360 listed for C means there are 360 C atoms in the dust for every 10^6 H atoms in the gas.

[b]Dust-phase abundances in grain cores + mantles are based on the abundances listed in Table 5 for the cool, diffuse clouds toward ζ Oph and ξ Per. The sources of the data are referenced in the footnotes to Table 5.

[c]Dust-phase abundances in grain cores are based on the average halo cloud abundances from Sembach & Savage (1996). The listed values of 10^6 (X/H)$_d$ refer mainly to atoms in the resilient cores of interstellar dust.

[d] Dust-phase abundances in grain mantles are derived by subtracting the listed dust core abundances from an average of the ζ Oph and ξ Per (core + mantle) abundances.

the form of H_2O, yields O/Si = 5 in the solid matter (see Fitzpatrick & Spitzer 1994). The abundances in primitive meteoric matter also appear to require the presence of O in the form of oxides.

CARBON Prior to the launch of the *HST*, reliable measures of the C abundance in diffuse interstellar clouds existed only for the sight line to δ Sco and were based on *Copernicus* satellite measurements of the very weak intersystem transition of C II] at 2325 Å (Hobbs et al 1982). The GHRS has provided measures of this weak line toward five stars: ζ Oph, ξ Per, ζ Per, λ Ori, and β^1 Sco (Cardelli et al 1996). The values of N(C II) obtained from the C II] λ2325 and damped C II λ1334 lines for ζ Oph and ξ Per agree to within 0.1 dex and confirm the reliability of the oscillator strength for the λ2325 line (Sofia et al 1994). The amount of C in the dust cores and mantles listed in Table 7 indicates a dust-phase abundance approximately a factor of two larger for ζ Oph than that for ξ Per. However, the gas-phase C abundances found for δ Sco, β^1 Sco, λ Ori, and ζ Per are similar to that found for ζ Oph, with an average result for these five stars of $10^6(\mathrm{C/H})_\mathrm{g} \approx 130$. This average implies that $10^6(\mathrm{C/H})_\mathrm{d} \approx 230$ and $10^6(\mathrm{C/H})_\mathrm{d} \approx 90$ for Solar and B-star reference abundances, respectively.

Many theories of the composition of interstellar dust (see Mathis 1996) require an appreciable amount of C in order to account for the 2175-Å (bump) absorption feature [$10^6(\mathrm{C/H})_\mathrm{d} \approx 50$] and for aspects of the continuous extinction [$10^6(\mathrm{C/H})_\mathrm{d} \approx 150$]. The polycyclic aromatic hydrocarbons are expected to use $10^6(\mathrm{C/H})_\mathrm{d} \approx 30$ (Tielens 1990). A total requirement of $10^6(\mathrm{C/H})_\mathrm{d} \approx 230$ in the dust is compatible with the GHRS average result for the five stars assuming solar abundances. However, for the B-star reference abundances and for the ξ Per measurement, the amount of C in the dust is not sufficient to explain the continuous extinction.

NITROGEN The observed gas-phase N abundances for the sight line to ζ Oph imply that little or no N is incorporated into interstellar grains (see Table 7). This result is supported by the fact that weak and damped N I line measurements yield similar N I column densities (Sofia et al 1994). It is also consistent with the expectation that N is unimportant in the formation of dust cores because the large activation energy of N_2 prevents it from participating in gas-phase reactions in stellar atmospheres that lead to dust formation (Gail & Sedlmayr 1986). Evidently, the gas-phase accretion of N onto grains in diffuse clouds is also impeded.

Mg, Fe, Si, Ni, Cr, Mn These elements have high degrees of incorporation into dust. Their relative dust-phase abundances are close to their cosmic abundances.

SULFUR Sulfur is found mainly in the gas phase.

THE RARER ELEMENTS The rare elements that have more than 70% of their atoms in dust [i.e. high depletion factor or (X/H) < -0.5] in the cool diffuse cloud toward ζ Oph include Li, B, Na, K, Ca, Ti, V, Co, Cu, Zn, Ga, Ge, and Pb (see Figure 4 and Table 5). Those that have significant gas-phase abundances [i.e. low depletion factor or (X/H) > -0.5] include P, Cl, Ar, As, Se, Kr, Sn, and Tl. Although we have yet to understand the exact behavior of all these elements in terms of various accretion and destruction processes, some interesting behaviors have been revealed. In particular, the subsolar gas-phase abundance of -0.3 dex for the noble gases Kr (Cardelli et al 1991a) and possibly Ar (Morton 1975) implies either incorrect reference abundances or the presence of noble gases in interstellar grains. GHRS abundance measurements for Kr are particularly secure because 1. the absorption line (Kr I λ1235) is weak, 2. the f-value is well determined, 3. the first ionization potential of 14.00 eV is close to that of H I, and 4. similar gas-phase abundances [(Kr/H) ≈ -0.26 dex] are measured for five sight lines with a wide range of conditions (Cardelli 1994). The estimate of the solar value of Kr/H is somewhat uncertain since it is based on meteoritic and solar wind data (Anders & Grevesse 1989).

The modest depletions of Kr and of various other heavy elements (Sn, Tl) may provide vital clues about the nucleosynthetic enrichment of the interstellar gas once some of the aforementioned reference abundance issues have been resolved. These elements are created through both slow and rapid nucleosynthetic processes and could yield information about advanced stages of nucleosynthetic enrichment in the Galaxy. Other heavy elements also may be useful in such studies once the degree of variation in gas-phase abundances resulting from incorporation into dust is better understood.

12.2 *Composition of Grain Cores*

By studying cloud-to-cloud variations in gas-phase abundances, Sembach & Savage (1996) determined that many interstellar clouds in low-density environments have similar depleted gas-phase abundances. In particular, interstellar clouds at moderate distances from the Galactic plane ($0.5 \leq |z| \leq 1.5$ kpc) have such regular gas-phase abundances that the dust in these clouds appears to have been stripped to a resilient core. If this interpretation is correct, the composition of those grain cores follows directly from the dust-phase composition inferred for halo clouds. The dust-phase abundances for the average of many halo clouds observed by Spitzer & Fitzpatrick (1993, 1995) and by Sembach & Savage (1996) are listed in Table 7.

Study of the relative dust-phase abundances of Mg, Fe, and Si in grain cores is interesting since the existence of silicate grains in the ISM is well established because of the detection of the 9.7- and 18.5-μm SiO stretch-and-bend features in absorption along sight lines with large extinctions (Roche & Aitken 1985).

The observed strength of these IR features requires that nearly all the interstellar Si must be in silicate grains (Draine & Lee 1984). The fact that these same features are also seen in emission toward cool highly evolved stars rich in O (Pégourié & Papoular 1985) suggests that the primary source of silicate grains in interstellar space may be mass ejection from cool stars. The two primary forms of silicate grain cores expected to be produced in stellar atmospheres and to occur in the ISM are pyroxene [(Mg, Fe)SiO_3] and olivine [$(Mg, Fe)_2SiO_4$] (Ossenkopf et al 1992). For pure pyroxene grain cores, the expected ratio of (Mg + Fe)/Si is 1.0, whereas the expected value for olivine cores is 2.0. From Table 7 we see that the implied value of (Mg + Fe)/Si for the grain cores in halo cloud dust is $(27 + 25)/16 = 3.3$ for solar reference abundances and $(12 + 13)/2.9 = 8.6$ for B-star reference abundances. In both cases the observations imply that an appreciable fraction of the Mg and Fe in these dust cores must exist in chemical forms that do not involve Si. Obvious candidate substances are oxides of Mg and Fe, including MgO, Fe_2O_3, and Fe_3O_4 (Nuth & Hecht 1990; Fadeyev 1988), and pure Fe. However, interstellar shock models imply a higher destruction rate for pure Fe grains compared with oxide grains, leading Sembach & Savage (1996) to suggest that the extra Mg and Fe atoms are more likely found in oxides (see Section 14).

If the Mg II $\lambda\lambda$1239, 1240 f-values from Hibbert et al (1983) are used instead of those recommended by Sofia et al (1994), the derived values of (Mg + Fe)/Si are $(0 + 25)/16 = 1.6$ and $(0 + 13)/2.9 = 4.5$ for solar and B-star reference abundances, respectively. Here, the case for oxide grains is less secure, and the implied grain core composition is consistent with Fe-bearing silicate grains (Spitzer & Fitzpatrick 1993, 1995).

Information about C, N, and O in grain cores is not available through halo cloud studies, but Meyer et al (1994) have shown that the interstellar gas-phase abundance of O is relatively constant over five decades in $f(H_2) = 2N(H_2)/[N(H\ I) + 2N(H_2)]$ (see Figure 2). This result suggests that the amount of O depleted from dense diffuse clouds such as those toward ζ Oph and ξ Per is similar to that depleted from the lower-density warm ISM sampled along low-reddening sight lines. For the short path through the local warm cloud to Capella, Linsky et al (1995) obtained $10^6(O/H)_g = 479$, which implies $10^6(O/H)_d = 260$ and $10^6(O/H)_d = 0.0$ for solar and B-star reference abundances, respectively.

12.3 *Composition of Grain Mantles*

If dust in clouds at large distances from the Galactic plane has the elemental composition of resilient grain cores, we can use that information to study the composition of grain mantles. The columns labeled mantle in Table 7 list the mantle composition obtained by subtracting the grain core composition from the average of the grain core + mantle entries for ζ Oph and ξ Per. For

both solar and B-star reference abundances, (Mg + Fe)/Si = (10 + 7)/18 = 0.94. The relative abundances of Mg, Fe, and Si in the mantles resemble those found in pyroxene [(Mg, Fe) SiO_3], provided the Mg II f-values are accurate. Regardless of the reference abundance chosen or the absolute value of the Mg II oscillator strengths, the cores and mantles of grains appear to differ significantly in composition.

13. ABUNDANCES IN HALO GAS

The study of elemental abundances in interstellar clouds at large distances from the Galactic plane has progressed rapidly since the launch of the *HST*. We draw heavily upon the work of Spitzer & Fitzpatrick (1993, 1995) and Sembach & Savage (1996) in presenting the basic results relevant to the gas- and dust-phase abundances in clouds in the low Galactic halo. In Figure 6 we show the average gas-phase abundance results for seven elements (S, Si, Mg, Mn, Cr, Fe, and Ni) detected in interstellar clouds at $|z| > 300$ pc toward two or more distant halo stars. For comparison, we also show the warm neutral medium gas-phase abundances for clouds in the Galactic disk (*crossed circles*) and for halo clouds having absorption blended with disk gas absorption (*open circles*). Average values for the cool diffuse disk clouds toward ξ Per and ζ Oph are shown as dotted circles.

From Figure 6 we see a clear progression toward increasing gas-phase abundance of these species from the disk to the halo. The abundance pattern is consistent with a more severe destruction of dust in the halo clouds than in the disk clouds. This destructive processing may result from either more frequent or more severe shocking of the halo clouds compared with the disk clouds. The GHRS results confirm, in a quantitative way, previous optical and *IUE* studies showing that the vertical Galactic scale heights of refractory elements (Ca, Ti, Fe) are larger than those of H I (Morton & Blades 1986; Edgar & Savage 1989; Sembach & Danks 1994; Lipman & Pettini 1995). Furthermore, the spread in the gas-phase abundances for individual halo clouds sampled for $R_g \approx 7$–10 kpc using the GHRS is less than 0.1 dex for Mg, Mn, Fe, and Ni and less than 0.15 dex for Si, S, and Cr, suggesting that the grain cores are difficult to destroy and do not deviate strongly in composition over widely different paths into the halo.

That dust cores with similar properties can survive at large distances from the Galactic plane is somewhat surprising since the transfer of gas into the halo is likely accomplished through supernova explosions in the disk. Models predict that only a few shocks with $v_{sh} \sim 100$ km s^{-1} would be necessary to liberate enough material from the grains to produce the diffuse halo cloud abundances shown in Figure 6 (Sembach & Savage 1996). Some support for this interpretation comes from direct comparisons of the halo cloud abundances with those in

strongly shocked environments, which indicate that the halo cloud abundances resemble those of intermediate- and high-velocity gas in the Vela supernova remnant (Jenkins & Wallerstein 1996). Still, the persistence of some types of grains in the ISM (such as the ultrasmall grains with radii < 10 Å) poses a problem for grain destruction and formation theories, partly because how material is cycled from one type of medium to another is unclear and partly because competing growth mechanisms cannot be distinguished from processing mechanisms without additional observations (see Draine 1990). Searches for the enrichment of Fe-peak elements (Fe, Ni) relative to α-process elements (Mg, Si) in halo gas by Type Ia supernovae at large distances from the Galactic plane suggest that the gas-transport processes that cycle material between the disk and the halo operate effectively on time scales short enough ($t \sim 10^7$–10^8 yr) to mask any vertical abundance gradients from S/N ejecta (Jenkins & Wallerstein 1996). These circulation processes include, but probably are not limited to, general turbulence in the disk, photolevitation of diffuse clouds, and movement of material by the flow of a Galactic fountain.

14. SHOCK DESTRUCTION OF GRAINS

It is generally accepted that shocks are responsible for most of the dust grain destruction in the ISM (Draine & Salpeter 1979a,b). Supernovae are likely the primary generators of these shocks in the disk and the halo of the Galaxy. A rich literature describes the effects of shocks on interstellar material and the consequences of such interactions (e.g. Bárlow 1978a,b; Shull & McKee 1979; Seab & Shull 1983; McKee et al 1987; Tielens et al 1994; Jones et al 1994; Vancura et al 1994). Recent reviews of the subject can be found in McKee (1989), Dwek & Arendt (1992), and Draine & McKee (1993).

The thermalization of supernova kinetic energy and the betatron acceleration of grains in the postshocked regions behind supernova blast waves lead to grain-grain collisions and sputtering (both thermal and nonthermal). These processes are most efficient in the warm neutral ISM, where the gas densities are moderate ($n_{\rm H} \sim 1$ cm^{-3}) and temperatures are high ($T \sim 10^4$ K) (see Draine & Salpeter 1979b; McKee et al 1987). Additional factors governing the destructiveness of shocks on grains include the porosity and mean molecular weight of the particles, the interstellar magnetic field strength, and partial grain vaporization (Jones et al 1994). Detailed models incorporating these (and many other) variables require high-quality data in order to test their validity and to place meaningful bounds on the range of possible postshock densities and temperatures. The halo cloud abundance measurements yield a ratio of (Mg + Fe)/Si $= 3.3 \pm 0.6$ for the chemical makeup of the grain cores (see Section 12), which is inconsistent with a pure silicate (olivine + pyroxene) composition for

which (Mg + Fe)/Si = 1.0–2.0, and indicates that there is probably another carrier of Fe in the dust besides silicates. As discussed in Section 12, possible carriers include a population of pure Fe grains or various Fe oxides. Shock models can be used to predict that pure Fe grains are destroyed more rapidly behind fast shocks than grains with lower mass densities (McKee et al 1987). We therefore reasonably can conclude that oxides are carriers of Fe since shocks generated by supernovae and cloud-cloud collisions within the Galactic disk are two likely mechanisms that eject gas and dust into the low halo of the Milky Way.

The abundance pattern for resilient grain cores in diffuse halo clouds derived through GHRS absorption-line measurements provides a reference point for the effectiveness of grain destruction and evolution considerations in models used in attempts to predict the emergent spectrum of shocked gas in interstellar environments. The composition of the halo cloud grain core indicates that localized enrichment of the gas behind a shock is probably most pronounced when the grain cores are destroyed. Grain destruction models suggest that large shock velocities are necessary in order to disrupt the cores completely (see Jones et al 1994). Observational studies of gas in supernova remnants may help show how elements are liberated into the gas phase by shocks. An example of variations in line strength with velocity has been given by Jenkins & Wallerstein (1995, 1996) for the interstellar direction toward HD 72089, which lies behind the Vela SNR. They found that absorption strengths of elements readily incorporated into dust grain, such as Al and Fe, increase by at least an order of magnitude relative to elements found mainly in gas, such as O and S, over the velocity range of ≈ 120 km s^{-1} spanned by absorption in the remnant. In particular, in the $+90$ to $+120$ km s^{-1} absorption toward HD 72089, the ratio of Fe to S is nearly solar (i.e. [Fe/S] ≈ 0) (see Figure 2 of Jenkins & Wallerstein 1995). The dependence of elemental depletion on cloud velocity was first documented by Routly & Spitzer (1952) on the basis of observations that the ratio of Ca II to Na I generally increased with increasing cloud velocity, presumably as a result of shock destruction of dust grains or changes in the ionization of the cloud (Routly & Spitzer 1952; Spitzer 1978 and references therein). Vallerga et al (1993) gave an excellent example of the effect for Ca II and Na I. UV observations with *Copernicus* and the GHRS, such as those for HD 72089, have extended the study of the velocity dependence of depletions to dominant ion stages and have made possible exploration of the physical conditions in the gas that give rise to the depletion changes.

15. ABUNDANCES IN HIGH-VELOCITY CLOUDS

The Milky Way is enveloped in H I high-velocity clouds (HVCs), which are detected in 21-cm emission with $|v_{\rm LSR}| \geq 100$ km s^{-1} (for a review see Wakker

1991). The nature and origin(s) of HVCs are poorly understood, but absorption-line abundance measurements are providing important new information about them. Table 8 lists the known optical and UV detections of heavy-element absorption lines associated with HVCs.

Optical observations from the ground have led to detections of Ca II toward many HVCs. Uncertainties associated with ionization corrections and the depletion of Ca prevent observers from obtaining direct information about the total Ca abundance in the HVCs. However, the Ca II observations confirm that the detected HVCs do not consist of primordial (metal-deficient) gas. In addition, ground-based observations of Ca II are crucial for setting constraints (usually upper limits) on the distances to the HVCs.

The GHRS and the Faint Object Spectrograph (FOS) have yielded measures of N(Mg II)/N(H I) toward a number of HVCs (Table 8). Many of the values are lower limits because the degree of absorption-line saturation is unknown. For the -209 and -147 km s^{-1} HVCs toward Mark 205, the footnotes to Table 8 explain how we estimated [Mg/H] from the equivalent widths reported by Bowen et al (1995).

Detailed information on abundances in a HVC is available for the $+240$ km s^{-1} gas toward the Seyfert galaxy NGC 3783 ($l = 287.5^\circ$, $b = +22.9^\circ$). Lu et al (1994a) detected the HVC in the lines of S II, Si II, and possibly C I with the GHRS in intermediate-resolution mode (20 km s^{-1} FWHM). Sulfur is the most useful element for deriving a metallicity for this HVC because it is not readily depleted onto interstellar dust and because the observed lines of S II are not saturated. Furthermore, S II (IP = 23.3 eV) should be the dominant ionization stage of S in the HVC, which has $N(\mathrm{H\ I}) = 1.21 \times 10^{20}$ cm^{-2}. Assuming the ionization corrections are not large, the observed measure of $N(\mathrm{S\ II})/N(\mathrm{H\ I}) = 2.8 \times 10^{-6}$ implies a gas-phase abundance relative to the Sun of $\delta(\mathrm{S}) = 0.15 \pm 0.05$. For the same cloud, the Si II λ1260 line is saturated and yields only a lower limit $\delta(\mathrm{Si}) \geq 0.006$. On the basis of these results, Lu et al (1994a) concluded that the HVC complex toward NGC 3783 is most likely associated with gas stripped from the Galaxy by an extragalactic object(s) such as the Magellanic Clouds.

The Seyfert galaxy Fairall 9 lies in the direction of the Magellanic Stream, which is an $\sim 180^\circ$ narrow band of H I extending from the Magellanic Clouds to the south Galactic pole and beyond. In the direction to Fairall 9 ($l = 295.1^\circ$, $b = -57.8^\circ$), the 21-cm emission associated with the Magellanic Stream reveals two components, one near $v_{\mathrm{LSR}} \approx +160$ km s^{-1}, with $N(\mathrm{H\ I}) \approx 2 \times 10^{19}$ cm^{-2} and the other at $v_{\mathrm{LSR}} \approx +200$ km s^{-1}, with $N(\mathrm{H\ I}) \approx 6 \times 10^{19}$ cm^{-2} (Morras 1983). Lu et al (1994b) used the GHRS to study the abundances of S II and Si II in these two clouds. S II was not detected, and Si II produced saturated absorption.

Table 8 H I-HVC metal line detections

Object	l (deg)	b (deg)	HVC	v_{LSR} (km s^{-1})	Ion	[X/H]	Reference[h]
Mark 106	161.1	42.9	Complex A	-157	Ca II	…[a]	1
I Zw 18	160.5	44.8	Complex A	-165	O I	> -1.57[f]	2
PG 1351+640	112.0	52.0	Complex C	-154	Ca II	…[a]	9
PG 1259+592	120.6	58.1	Complex C	-127	Mg II	…[b]	3
Mark 205	125.4	41.7	125+41-209	-209	Mg II	-2.24$_{(+0.31,-0.05)}$[c,e]	4
"	"	"	Complex C	-147	Mg II	-0.59$_{(+1.09,-0.38)}$[c,e]	4
Mark 290	91.5	47.9	Complex C	-138	Ca II	…[a]	9
3C351	90.1	36.4	Complex C	-180	Mg II	…[b]	3
BD +38 2182	182.2	62.2	Complex M	-90	Si II	> -0.80[c]	5
"	"	"	Complex M	-96	Ca II	…[a]	13
PG 0043+039	120.2	-58.7	Mag. Stream	-348	Mg II	> -0.92[c]	3
PKS 2251+11	82.8	-41.9	Mag. Stream	-374	Mg II	> -1.23[c]	3
3C 454.3	86.1	-38.2	Mag. Stream	-397	Mg II	> -0.49[c]	3
Fairall 9	295.1	-57.8	Mag. Stream	+195	Ca II	…[a]	10
"	"	"	Mag. Stream	+160	Si II	> -0.70[c]	6
"	"	"	Mag. Stream	+200	Si II	> -1.15[c]	6
Q0637-752	286.4	-27.2	Outer Galaxy	+125	Mg II	…[g]	14
PKS 0837-12	237.2	17.4	242+17+106	+105	Ca II	…[a]	11
NGC 3783	287.5	23.0	287+22+240	+240	Ca II	…[a]	12
"	"	"	287+22+240	+240	S II	-0.82$_{(+0.12,-0.18)}$	7
"	"	"	287+22+240	+240	Si II	> -2.22[c]	7
H1821+643	94.0	27.4	Outer Arm	+120	Si II	~ -1.0:[c,d]	8
"	"	"	Outer Arm	+120	Mg II	~ -1.0:[c,d]	8

[a]Abundances have not been derived from the Ca II observations since ionization corrections and Ca depletion into dust grains make any such measures uncertain.

[b]Detection is from FOS measurements. Strong blending with lower-velocity gas prevents reliable measure of absorption-line strength for the HVC alone.

[c]Result may be influenced by the effects of dust depletion.

[d]Value uncertain. A large correction for the effects of ionization by the extragalactic background is required (see Savage et al 1995).

[e]The numbers listed for the Mg abundances in the HVCs toward Mark 205 are calculated from the revised Mg II equivalent widths listed by Bowen et al (1995), from the curve-or-growth error method of Savage et al (1990), and from the values of N(H I) from Lockman & Savage (1995). The values of log N(Mg II) $\pm 1\sigma$ obtained for the clouds at -209 and -147 km s^{-1} are 12.62 ($+0.3$, -0.05) and 13.14 ($+1.09$, -0.38), respectively. The errors for N(Mg II) associated with the cloud at -147 km s^{-1} are much larger than suggested by the formal profile fit results of Bowen & Blades (1993). The -147 km s^{-1} cloud also has a poorly determined value of N(H I).

[f]The uncertain O I equivalent width for the HVC toward I Zw 18 obtained by Kunth et al (1994) has been used to estimate a lower limit for N(O I), assuming the observed absorption is produced on the linear part of the curve of growth. The listed limit for [O/H] follows from N(H I) $= 2.1 \times 10^{19}$ cm^{-2} (Kunth et al 1994). We do not list a result for Si II since the feature reported for the Si II λ1304 line has less than 2σ significance.

[g]Bowen et al (1995) detected Mg II absorption toward Q0637-752 in the velocity range from $+100$ to $+150$ km s^{-1}. These authors attribute the high-velocity gas to corotating high $|z|$ gas in the outer galaxy. Mg II and H I column densities are not reported. Note that gas at similar velocities is seen toward many stars in the Large Magellanic Cloud in the direction $l \approx 279^\circ$, $b \approx -32^\circ$ (Savage & de Boer 1981).

[h]References: (1) Schwarz et al 1995; (2) Kunth et al 1994; (3) Savage et al 1993a; (4) Bowen & Blades 1993, Bowen et al 1995; (5) Danly et al 1993; (6) Lu et al 1994b, upper limits also reported for S II; (7) Lu et al 1994a; (8) Savage et al 1995; (9) Wakker et al 1996; (10) Songaila 1981; (11) Robertson et al 1991; (12) West et al 1985; (13) Keenan et al 1995; (14) Bowen et al (1995).

Assuming the ionization corrections are not large, the observations show that $\delta(\mathrm{Si}) \geq 0.2$ and $\delta(\mathrm{S}) \leq 0.9$ for the $+160$ km s^{-1} HVC and that $\delta(\mathrm{Si}) \geq 0.07$ and $\delta(\mathrm{S}) \leq 0.3$ for the $+200$ km s^{-1} HVC. These limits are consistent with an origin for the Magellanic Stream closely tied to gas in the Magellanic Clouds.

UV absorption-line measurements of abundant species provide an estimate of the sky-covering factor of high-velocity gas with $|v_{\mathrm{LSR}}| > 100$ km s^{-1} containing metals. The first results based on FOS 300-km s^{-1} resolution spectra of quasars (Savage et al 1993a) revealed that 6 of 14 sight lines exhibited high-velocity Mg II absorption, excluding H1821 + 643, which has high-velocity absorption associated with the Galactic warp. Two of the seven extragalactic sight lines studied by Bowen et al (1995) have high-velocity absorption: Mark 205 and the $+100$ to $+150$ km s^{-1} absorption toward Q0637-752. When the two data sets are combined, 8 of 21 extragalactic sight lines exhibit high-velocity Mg II absorption. This observation suggests a high-velocity Mg II sky-covering factor of $38 \pm 13\%$. Although this result is still subject to large errors owing to the small sample size, it is consistent with the large sky-covering factor of 37% for H I HVCs recently detected by Murphy et al (1995) through a sensitive HVC 21-cm emission line search. These authors found a large population of low–column density HVCs with $7 \times 10^{17} < N(\mathrm{H\ I}) < 2 \times 10^{18}$ cm^{-2} not detected in earlier surveys. Virtually all newly detected high-velocity, 21-cm emission is associated with previously known emission complexes, which evidently have extensive low–column density outer envelopes.

Highly ionized HVCs also have been discovered in spectra obtained by the GHRS. For example, they have been observed in the C IV doublet toward Mark 509 (Sembach et al 1995a) PKS 2155-304 (Bruhweiler et al 1993). In the direction of Mark 509, the C IV absorption extending from -170 to -340 km s^{-1} appears to be associated with H I-HVCs at similar velocities 1.5° from the line of sight. Sembach et al (1995a) favor the interpretation that this C IV-HVC is the low-density photoionized boundary of the H I-HVC. However, an origin in collisionally ionized gas with $T > 10^5$ K cannot be eliminated without further observations.

ACKNOWLEDGMENTS

The ISM abundance results discussed in this review would not have been obtained without the dedicated efforts of the many people responsible for the construction, launch, and operation of the *HST*, GHRS, and FOS. We thank them all. We appreciate comments on draft versions of our review by Steve Federman, Edward Jenkins, John Mathis, David Meyer, Todd Tripp, Alan Sandage, Lyman Spitzer, and Bart Wakker. We also thank Edward Fitzpatrick for providing an electronic version of Figure 1 and Jason Cardelli for providing the C II]

data in Figure 3. KRS acknowledges support from a Hubble Fellowship from NASA through Grant number HF-1038.01-92A from the Space Telescope Science Institute, which is operated by AURA under NASA contract NAS5-26555. BDS appreciates support from NASA Grant NAG5-1852.

Literature Cited

Aldrovandi SMV, Péquignot D. 1973. *Astron. Astophys.* 25:137–40
Aldrovandi SMV, Péquignot D. 1974. *Rev. Bras. Fis.* 4:491
Aldrovandi SMV, Péquignot D. 1976. *Asron. Astrophys.* 47:321 (Erratum)
Anders E, Grevesse N. 1989. *Geochim. Cosmochim. Acta* 53:197–214
Barlow MJ. 1978a. *MNRAS* 183:367–95
Barlow MJ. 1978b. *MNRAS* 183:397–415
Barlow MJ, Silk J. 1977. *Ap. J.* 215:800–4
Bergeson SD, Lawler JE. 1993a. *Ap. J.* 408:382–88
Bergeson SD, Lawler JE. 1993b. *Ap. J. Lett.* 414:L137–40
Bergeson SD, Mullman KL, Lawler JE. 1994. *Ap. J. Lett.* 435:L157–59
Bergeson SD, Mullman KL, Wickliffe ME, Lawler JE. 1996a. *Ap. J. Lett.*, In press
Bergeson SC, Mullman KL, Lawler JE. 1996b. *Ap. J. Lett.* In press
Blades JC, Wynne-Jones I, Wayte RC. 1980. *MNRAS* 193:849–66
Bohlin RC. 1975. *Ap. J.* 200:402–14
Borkowski KJ, Balbus SA, Fristrom CC. 1990. *Ap. J.* 355:501–17
Bosegaard AM, Heacox WD. 1978. *Ap. J.* 226:888–96
Bowen D, Blades JC. 1993. *Ap. J. Lett.* 403:L55–58
Bowen D, Blades JC, Pettini M. 1995. *Ap. J.* 448:662–66
Brage T, Leckrone DJ. 1995. *J. Phys. B* 28:1201–10
Brandt JC, Heap SR, Beaver EA, Boggess A, Carpenter KG, et al. 1994. *Publ. Astron. Soc. Pac.* 106:890–908
Bregman JN, Harrington JP. 1986. *Ap. J.* 309:833–45
Bruhweiler FC, Boggess A, Norman DJ, Grady CA, Urry M, Kondo Y. 1993. *Ap. J.* 409:199–204
Bruhweiler FC, Cheng KP. 1988. *Ap. J.* 355:188–96
Bruston P, Audouze J, Vidal-Madjar A, Laurent C. 1981. *Ap. J.* 243:161–69
Calamai AG, Smith PL, Bergeson SD. 1993. *Ap. J. Lett.* 415:L59–62
Cappa de Nicolau CE, Poppel WGL. 1986. *Astron. Astrophys.* 164:274–99
Cardell JA. 1994. *Science* 265:209–13
Cardelli JA, Ebbets DC. 1994. In *Calibrating Hubble Space Telescope*, ed. JC Blades, SJ Osmer, pp. 322–31. Baltimore: Space Telesc. Sci. Inst.
Cardelli JA, Ebbets DC, Savage BD. 1993a. *Ap. J.* 413:401–15
Cardelli JA, Federman SR, Lambert DL, Theodosiou CE. 1993b. *Ap. J. Lett.* 416:L41–44
Cardelli JA, Mathis JS, Ebbets DC, Savage BD. 1993c. *Ap. J. Lett.* 402:L17–20
Cardelli JA, Meyer DM, Jura M, Savage BD. 1996. *Ap. J.* In press
Cardelli JA, Savage BD, Ebbets DC. 1991a. *Ap. J. Lett.* 383:L23–28
Cardelli JA, Savage BD. 1995. *Ap. J.* 452:275–85
Cardelli JA, Savage BD, Bruhweiler FC, Smith AM, Ebbets DC, et al. 1991b. *Ap. J. Lett.* 377:L57–60
Cardelli JA, Sembach KR, Savage BD. 1995. *Ap. J.* 440:241–53
Cardelli JA, Sofia UJ, Savage BD, Keenan FP, Dufton PL. 1994. *Ap. J. Lett.* 420:L29–32
Cassinelli JP, Cohen DH, MacFarlane JJ, Drew JE, Lynas-Gray AE, et al. 1995. *Ap. J.* 438:932–49
Clarke JT, Lallement R, Berteaux J-L, Quemerais R. 1995. *Ap. J.* 448:893–904
Crane P, Hegyi DJ, Lambert DL. 1991. *Ap. J.* 378:181–85
Cowie LL, Songaila A. 1986. *Annu. Rev. Astron. Astrophys.* 24:499–535
Crinklaw G, Federman SR, Joseph CL. 1994. *Ap. J.* 424:748–53
Danly L, Albert CE, Kuntz KD. 1993. *Ap. J. Lett.* 416:29–32
Dar A. 1995. *Ap. J.* 449:550–53

de Boer KS, Jura MA, Shull JM. 1987. See Kondo 1987, pp. 533–59
de Boer KS, Koppenaal K, Pottasch SR. 1973. *Astron. Astrophys.* 28:145–46
Diplas A, Savage BD. 1994. *Ap. J. Suppl.* 93:211–28
Dömgorgen H, Mathis JS. 1994. *Ap. J.* 428:647–53
Dove JB, Shull JM. 1994. *Ap. J.* 430:222–35
Draine BT. 1978. *Ap. J. Suppl.* 36:595–619
Draine BT. 1990. In *Evolution of the Interstellar Medium*, ed. L Blitz, pp. 193–205. San Francisco: Astron. Soc. Pac. Conf. Ser. Vol. 12
Draine BT, Lee HM. 1984. *Ap. J.* 285:89–108
Draine BT, McKee CF. 1993. *Annu. Rev. Astron. Astrophys.* 31:373–432
Draine BT, Salpeter EE. 1979a. *Ap. J.* 231:77–94
Draine BT, Salpeter EE. 1979b. *Ap. J.* 231:438–55
Dufour RJ. 1987. See Kondo 1987, pp. 577–87
Dufton PL, Hibbert A, Kingston AE, Tully JA. 1983. *MNRAS* 202:145–50
Dufton PL, Keennan FP, Hibbert A, Ojha PC, Stafford RP. 1992. *Ap. J.* 387:414–16
Dwek E, Arendt RG. 1992. *Annu. Rev. Astron. Astrophys.* 30:11–50
Edgar RJ, Savage BD. 1989. *Ap. J.* 340:762–74
Fang Z, Kwong VHS, Wang J, Parkinson WH. 1993. *Phys. Rev. A* 48:1114–22
Fadeyev Y. 1988. In *Atmospheric Diagnostics of Stellar Evolution*, ed. K Nomoto, pp. 174–80. Berlin: Springer-Verlag
Federman SR, Beideck DJ, Schectman RM, York DG. 1992. *Ap. J. Lett.* 401:367–70
Federman SR, Cardelli JA. 1995. *Ap. J.* 452:269–74
Federman SR, Cardelli JA, Sheffer Y, Lambert DL, Morton DC. 1994. *Ap. J. Lett.* 432:L139–42
Federman SR, Cardelli JA, van Dishoeck EF, Lambert DL, Black JH. 1995. *Ap. J.* 445:325–29
Federman SR, Sheffer Y, Lambert DL, Gilliland RL. 1993. *Ap. J. Lett.* 413:L51–54
Field G. 1974. *Ap. J.* 187:453–59
Fitzpatrick EL, Spitzer L. 1994. *Ap. J.* 427:232–58
Fitzsimmons A, Brown PJF, Dufton PL, Lennon DJ. 1990. *Astron. Astrophys.* 232:437–42
Foltz CB, Chaffee CB, Frederic H Jr, Black JH. 1988. *Ap. J.* 324:267–78
Frisch PC. 1994. *Science* 265:1423–27
Frisch PC, Jura MJ. 1980. *Ap. J.* 242:560–67
Frisch PC, Welty DE, York DG, Fowler JR. 1990. *Ap. J.* 357:514–23
Fuhr JR, Wiese WL. 1991. In *Atomic Transition Probabilities*, ed. DR Lide, pp. 10–128. *CRC Handbook of Chemistry and Physics*. Cleveland: CRC Press. 72nd ed.
Gail H, Sedlmayr E. 1986. *Astron. Astrophys.* 166:225–36
Gies DR, Lambert DL. 1992. *Ap. J.* 387:673–700
Gondhalekar PM, Wilson R. 1975. *Astron. Astrophys.* 38:329–33
Gould RJ. 1978. *Ap. J.* 219:250–61
Grevesse N, Noels A. 1993. In *Origin of the Elements*, ed. N Prantzos, E Vangioni-Flam, M Cassé, pp. 15–25. Cambridge: Cambridge Univ. Press
Gry C, Lemonon L, Vidal-Madjar A, Lemoine M, Ferlet R. 1995. *Astron. Astrophys.* 302:497–508
Grossman L, Larimer JW. 1974. *Rev. Geophys. Space Phys.* 12:71–101
Harris AW, Bromage GE. 1984. *MNRAS* 208:941–53
Harris AW, Mas Hesse JM. 1986. *MNRAS* 220:271–78
Hawkins I, Craig N, Meyer DM. 1993. *Ap. J.* 407:185–97
Heap SR, Brandt J, Randall CE, Carpenter KG, Leckrone DS, et al. 1995. *Pub. Astron. Soc. Pac.* 107:871–87
Hibbert A, Dufton PL, Murray MJ, York DG. 1983. *MNRAS* 205:535–41
Hobbs LM, York DG, Oegerle W. 1982. *Ap. J. Lett.* 252:L21–23
Hobbs LM, Welty DE, Morton DC, Spitzer L, York DG. 1993. *Ap. J.* 411:750–55
Huang J-S, Songaila A, Cowie LL, Jenkins EB. 1995. *Ap. J.* 450:163–78
Jenkins EB. 1987. In *Interstellar Processes*, ed. DJ Hollenbach, HA Thronson, pp. 533–59. Dordrecht: Reidel
Jenkins EB. 1990. In *Evolution in Astrophysics: IUE Astronomy in the Era of New Space Missions*, Vol. Sp-310, pp. 133–41. Noordwijk: ESA
Jenkins EB. 1995. In *Laboratory and Astronomical High Resolution Spectra*, ed. AJ Sauval, R Blomme, N Grevesse, pp. 453–58. San Francisco: Astron. Soc. Pac. Conf. Ser. Vol. 81
Jenkins EB, Drake FJ, Morton DC, Rogerson JB, Spitzer L, York DG. 1973. *Ap. J.* 181:L122–27
Jenkins EB, Joseph CL, Long D, Zucchino PM, et al. 1988. *Proc. SPIE* 932:213–29
Jenkins EB, Lees JF, van Dishoeck EF, Wilcots EM. 1989. *Ap. J.* 343:785–810
Jenkins EB, Savage BD, Spitzer L. 1986. *Ap. J.* 301:355–79
Jenkins EB, Wallerstein G. 1995. *Ap. J.* 440:227–40
Jenkins EB, Wallerstein G. 1996. *Ap. J.* In press
Jones AP, Tielens AGGM, McKee CF, Hollenbach DJ. 1994. *Ap. J.* 433:797–810

Joseph CL. 1988. *Ap. J.* 335:157–67
Joseph CL, Jenkins EB. 1991. *Ap. J.* 368:201–14
Jura M. 1974. *Ap. J.* 191:375–79
Jura M, Meyer DM, Hawkins I, Cardelli JA. 1996. *Ap. J.* 456:598–601
Keenan FP, Shaw CR, Bates B, Dufton PL, Kemp SN. 1995. *MNRAS* 272:599–604
Kilian-Montenbruck J, Gehren T, Nissen PE. 1994. *Astron. Astrophys.* 291:757–64
Kingdon JB, Ferland GJ. 1995. *Ap. J.* 450:691–704
Kondo Y, ed. 1987. *Exploring the Universe with the IUE Satellite*. Dordrecht: Reidel
Köppen J, Aller LH. 1987. See Kondo 1987, pp. 589–602
Kunth D, Lequeux J, Sargent WLW, Viallefond F. 1994. *Astron. Astrophys.* 282:709–16
Lallement R, Bertin P, Ferlet R, Vidal-Madjar A, Bertaux JL. 1994. *Astron. Astrophys.* 286:898–908
Lambert DL, Sheffer Y, Federman SR. 1995. *Ap. J.* 438:740–49
Lambert DL, Sheffer Y, Gilliland RL, Federman SR. 1994. *Ap. J.* 420:756–71
Lancet MS, Anders E. 1973. *Geochim. Cosmochim. Acta* 37:1371–88
Laurent C, Vidal-Madjar A, York DG. 1979. *Ap. J.* 229:923–41
Lemke M, Lambert DL, Edvardsson B. 1993. *Publ. Astron. Soc. Pac.* 105:468–75
Lennon DJ, Dufton PL, Fitzsimmons A, Gehren T, Nissen PE. 1990. *Astron. Astrophys.* 240:349–56
Lennon DJ, Dufton PL, Hibbert A, Kingston AE. 1985. *Ap. J.* 294:200–6
Levshakov S, Chaffee FH, Foltz CB, Black JH. 1992. *Astron. Astrophys*. 262:385–94
Linsky JL, Brown A, Gayley K, Diplas A, Savage BD, et al. 1993. *Ap. J.* 402:694–709
Linsky JL, Diplas A, Wood BE, Brown A, Ayres TR, Savage BD. 1995. *Ap. J.* 451:335–51
Lipman K, Pettini M. 1995. *Ap. J.* 442:628–37
Lockman FJ, Savage BD. 1995. *Ap. J. Suppl.* 97:1–47
Lu L, Savage BD, Sembach KR. 1994a. *Ap. J.* 426:563–76
Lu L, Savage BD, Sembach KR. 1994b. *Ap. J. Lett.* 437:L119–22
Lyu C-H, Smith AM, Bruhweiler FC. 1994. *Ap. J.* 426:254–68
Mathis JS. 1987. See Kondo 1987, pp. 517–29
Mathis JS. 1990. *Annu. Rev. Astron. Astrophys.* 28:37–70
Mathis JS. 1995. *Rev. Mex. Astron. Astrophys.* Serie de conf. 3:207–14
Mathis JS. 1996. In *Polarimetry of the Interstellar Medium*, ed. W Roberge, DCCM Whittet. San Francisco: Astron. Soc. Pac. In press
McCullough PR. 1992. *Ap. J.* 390:213–18
McKee CF. 1989. In *IAU Symp. 135: Interstellar Dust*,. ed. LJ Allamandola, AGGM Tielens, pp. 431–44. Dordrecht: Kluwer
McKee CF. 1993. In *Back to the Galaxy*, ed. S Holt, F Verter, pp. 499–513. New York: Am. Inst. Phys.
McKee CF, Hollenback DJ, Seab CG, Tielens AGGM. 1987. *Ap. J.* 318:674–701
Mendoza C. 1992. In *Atomic and Molecular Data for Space Astronomy: Needs, Analysis, and Availability, Lecture Notes in Physics*. ed. PL Smith, WL Wiese, pp. 85–119. Berlin: Springer-Verlag
Meyer DM, Jura MJ, Hawkins I, Cardelli JA. 1994. *Ap. J. Lett.* 437:L59–61
Miller WW, Cox DP. 1993. *Ap. J.* 417:579–94
Moore CE. 1970. *Ionization Potentials and Ionization Limits Derived from the Analysis of Optical Spectra. Rep. No. NSRDS-NBS34*. Washington, DC: US Dept. Commerce
Morras R. 1983. *Astron. J.* 88:62–66
Morton DC. 1975. *Ap. J.* 197:85–115
Morton DC. 1991. *Ap. J. Suppl.* 77:119–202
Morton DC, Blades JC. 1986. *MNRAS* 220:927–48
Morton DC, Noreau L. 1994. *Ap. J. Suppl.* 95(1):301–43
Morton DC, Spitzer L. 1966. *Ap. J.* 144:1–12
Murphy E, Lockman FJ, Savage BD. 1995. *Ap. J.* 447:642–45
Murray MJ, Dufton PL, Hibbert A, York DG. 1984. *Ap. J.* 282:481–84
Nussbaumer H, Storey PJ. 1983. *Astron. Astrophys*. 126:75–79
Nussbaumer H, Storey PJ. 1984. *Astron. Astrophys. Suppl*. 56:293–312
Nussbaumer H, Storey PJ. 1986. *Astron. Astrophys. Suppl*. 64:545–55
Nuth JA, Hecht JH. 1990. *Astrophys. Space Sci*. 163:79–94
Ossenkopf V, Henning Th, Mathis JS. 1992. *Astron. Astrophys.* 261:567–78
Pégourié B, Papoular R. 1985. *Astron. Astrophys*. 142:451–60
Peimbert M. 1995. In *Analysis of Emission Lines*, ed RE Williams. Cambridge: Cambridge Univ. Press. In press
Peimbert M, Torres-Peimbert S, Dufour RJ. 1993. *Ap. J.* 413:242–50
Péquignot D, Aldrovandi SMV. 1986. *Astron. Astrophys.* 161:169–76
Péquignot D, Boisson C, Pettijean P. 1991. *Astron. Astrophys*. 252:680–88
Reilman RF, Manson ST. 1979. *Ap. J. Suppl.* 40:815–80
Reynolds RJ. 1993. In *Back to the Galaxy*, ed. S Holt, F Verter, pp. 156–65. New York: Am. Inst. Phys.
Ripken HW, Fahr HJ. 1983. *Astron. Astrophys*. 122:181–92

Robertson JG, Morton DC, Schwarz UJ, van Woerden H, Murray D. 1991. *MNRAS* 248:508–14
Roche PF, Aitken DK. 1985. *MNRAS* 215:425–35
Rolleston WRJ, Brown PJF, Dufton PL, Fitzsimmons A. 1993. *Astron. Astrophys.* 270:107–16
Rolleston WRJ, Dufton PL, Fitzsimmons A. 1994. *Astron. Astrophys.* 284:72–81
Rogerson JB, York DG. 1973. *Ap. J. Lett.* 186:L95–98
Rogerson JB, York DG, Drake FJ, Jenkins EB, Morton DC, Spitzer L. 1973. *Ap. J. Lett.* 181:L110–15
Roth K, Blades JC. 1995. *Ap. J. Lett.* 445:L95–98
Routly PMcR, Spitzer L. 1952. *Ap. J.* 115:227–43
Sandford SA, Allamandola LJ, Tielens AGGM, Sellgren K, Tapia M, Pendleton Y. 1991. *Ap. J.* 371:607–20
Sargent WLW, Young PJ, Bocksenberg A, Carswell RF, Whelan JAJ. 1979. *Ap. J.* 230:49–67
Savage BD, Bohlin RC. 1979. *Ap. J.* 229:136–46
Savage BD, Bohlin RC, Drake JF, Budich W. 1977. *Ap. J.* 216:291–307
Savage BD, Cardelli JA, Bruhweiler FC, Smith AM, Ebbets DC, Sembach KR. 1991. *Ap. J. Lett.* 377:L53–56
Savage BD, Cardelli JA, Sofia UJ. 1992. *Ap. J.* 401:706–23
Savage BD, de Boer KS. 1981. *Ap. J.* 243:460–84
Savage BD, Edgar RJ, Diplas A. 1990. *Ap. J.* 361:107–15
Savage BD, Jeske NA. 1981. *Ap. J.* 244:768–76
Savage BD, Lu L, Bahcall JN, Bergeron J, Boksenberg A, et al. 1993a. *Ap. J.* 413:116–36
Savage BD, Lu L, Weymann RJ, Morris SL, Gilliland RL. 1993b. *Ap. J.* 404:124–43
Savage BD, Sembach KR. 1991. *Ap. J.* 379:245–59
Savage BD, Sembach KR. 1994. *Ap. J.* 434:145–61
Savage BD, Sembach KR, Cardelli JA. 1994. *Ap. J.* 420:183–96
Savage BD, Sembach KR, Lu L. 1995. *Ap. J.* 449:145–55
Schattenburg ML, Canizares CR. 1986. *Ap. J.* 301:759–71
Schectman RM, Federman SR, Beideck DJ, Ellis DG. 1993. *Ap. J.* 406:735–38
Schwarz UJ, Wakker BP, van Woerden H. 1995. *Astron. Astrophys.* 302:364–81
Seab CG, Shull MJ. 1983. *Ap. J.* 275:652–60
Seaton MJ, Zeippen CJ, Tully JA, et al. 1992. *Rev. Mex. Astron. Astrophys.* 23:19–43
Sembach KR, Danks AC. 1994. *Astron. Astrophys.* 289:539–58
Sembach KR, Savage BD. 1992. *Ap. J. Suppl.* 83:147–201
Sembach KR, Savage BD. 1994. *Ap. J.* 431:201–22
Sembach KR, Savage BD. 1996. *Ap. J.* 457:211–27
Sembach KR, Savage BD, Jenkins EB. 1994. *Ap. J.* 421:585–99
Sembach KR, Savage BD, Lu L, Murphy EM. 1995a. *Ap. J.* 451:616–23
Sembach KR, Steidel CC, Macke R, Meyer DM. 1995b. *Ap. J.* 445:L27–30
Shapiro PR, Benjamin RA. 1993. In *Star-Forming Galaxies and Their Interstellar Media*, ed. JJ Franco. Dordrecht: Reidel
Shull MJ, McKee CM. 1979. *Ap. J.* 227:131–49
Shull MJ, van Steenberg ME. 1985. *Ap. J.* 294:599–614
Slavin JD. 1989. *Ap. J.* 346:718–27
Slavin JD, Shull JM, Begelman MC. 1993. *Ap. J.* 407:83–99
Smith AM, Bruhweiler FC, Lambert DL, Savage BD, Cardelli JA, et al. 1991. *Ap. J. Lett.* 377:L61–64
Snow TP, Black JH, van Dishoeck EF, Burks G, Crutcher RM, Lutz BL, Hanson MM, & Shuping RY. 1996. *Ap. J.* In press
Soderblom DR, Gonnella A, Hulbert SJ, Leitherer C, Schultz A. 1995. *Instrument Handbook for the Goddard High Resolution Spectrograph*, Version 6.0. Baltimore: Space Telesc. Sci. Inst.
Sofia UJ, Cardelli JA, Savage BD. 1994. *Ap. J.* 430:650–66
Sofia UJ, Savage BD, Cardelli JA. 1993. *Ap. J.* 413:251–67
Songaila A. 1981. *Ap. J. Lett.* 243:L19–22
Songaila A, Cowie LL, Hogan CJ, Rugers M. 1994. *Nature* 368:599–604
Spitzer L. 1978. *Physical Processes in the Interstellar Medium*. New York: Wiley
Spitzer L. 1985. *Ap. J. Lett.* 290:L21–24
Spitzer L. 1990. *Annu. Rev. Astron. Astrophys.* 28:71–101
Spitzer L, Cochran WD, Hirshfeld A. 1974. *Ap. J. Suppl.* 28:373–89
Spitzer L, Jenkins EB. 1975. *Annu. Rev. Astron. Astrophys.* 13:133–64
Spitzer L, Fitzpatrick EL. 1992. *Ap. J. Lett.* 391:L41–44
Spitzer L, Fitzpatrick EL. 1993. *Ap. J.* 409:299–318
Spitzer L, Fitzpatrick EL. 1995. *Ap. J.* 445:196–210
Steidel CC. 1990. *Ap. J. Suppl.* 74:37–91
Stokes GM. 1978. *Ap. J. Suppl.* 36:115–41
Tripp T, Cardelli JA, Savage BD. 1994. *Astron. J.* 107:645–50

Tielens AGGM. 1990. In *Submillimeter and Millimeter Astronomy*, ed. G Watt, A Webster, pp. 13–17. Dordrecht: Kluwer
Tielens AGGM, McKee CF, Seab CG, Hollenbach DJ. 1994. *Ap. J.* 431:321–40
Vallerga JV, Welsh BY. 1995. *Ap. J.* 444:702–7
Vallerga JV, Vedded PW, Craig N, Welsh BY. 1993. *Ap. J.* 411:729–49
Vancura O, Raymond JC, Dwek E, Blair WP, Long KS, Foster S. 1994. *Ap. J.* 431:188–200
van Dishoeck EF, Black JH. 1986. *Ap. J. Suppl.* 62:109–45
Verner D, Barthel P, Tytler D. 1994. *Astron. Astrophys. Suppl.* 108:287–340
Wakker BP. 1991. In *IAU Symp. 144: The Interstellar Disk-Halo Connection in Galaxies*, ed. H Bloemen, pp. 27–40. Dordrecht: Kluwer
Wakker BP, van Woerden H, Schwarz UJ, Peletier RF, Douglas N. 1996. *Astron. Astrophys.* Submitted
Wallerstein G, Vanture AD, Jenkins EB. 1995a. *Ap. J.* 455:590–97
Wallerstein G, Vanture AD, Jenkins EB, Fuller GM. 1995b. *Ap. J.* 449:688–94
Walker TP, Steigman G, Schramm DN, Olive KA, Kang H-S. 1991. *Ap. J.* 376:51–69
Wai CM, Wasson JT. 1977. *Earth Planet. Sci. Lett.* 36:1–13
Wasson JT. 1985. *Meteorites: Their Record of the Early Solar System History.* New York: Freeman
Wasson JT, Kallemeyn GW. 1988. *Philos. Trans. R. Soc. London Ser. A* 325:535–44
Wayte RC, Wynne-Jones I, Blades JC. 1978. *MNRAS* 182:5P–10P
Welty DE, Hobbs LM, Kulkarni VP. 1994. *Ap. J.* 436:152–75
Welty DE, Hobbs LM, Lauroesch JT, Morton DC, York DG. 1995. *Ap. J. Lett.* 449:L135–38
West KA, Pettini M, Penston M, Blades JC, Morton DC. 1985. *MNRAS* 215:481–97
Whittet DCB. 1984. *MNRAS* 210:479–87
Whittet DCB. 1992. *Dust in the Galactic Environment*. New York: Inst. Phys.
Wilson TL, Rood RT. 1994. *Annu. Rev. Astron. Astrophys.* 32:191–226
Witt AN, Johnson MW. 1973. *Ap. J.* 181:363–68
York DG, Kinahan BF. 1979. *Ap. J.* 228:127–46
York DG, Rogerson JB. 1976. *Ap. J.* 203:378–85
York DG, Spitzer L, Bohlin RC, Hill J, Jenkins EB, et al. 1983. *Ap. J. Lett.* 265:L55–59